Development of a Novel Fistula Occlusion Device

By

Alyssa Kirk Rollando

Submitted to the graduate degree program in BioEngineering and the Graduate Faculty of the University of Kansas in partial fulfillment of the requirements for the degree of Master of Science.

_____

Chairperson, Dr. Sara Wilson

_____

Dr. James Stiles

_____

Dr. Stephen Waller

_____

Dr. Richard Gilroy

Date Defended: April 25, 2016

The Thesis Committee for Alyssa Rollando

certifies that this is the approved version of the following thesis:

Development of a Novel Fistula Occlusion Device

_____

Chairperson Dr. Sara Wilson

Date approved: April 25, 2016

# Abstract

Fistulas are a pathological tunnel between two hollow organs or an organ and the skin. There is currently no gold-standard for treatment as invasive surgical procedures carry significant morbidity, and potential for failure; many patients are also not surgical candidates due to comorbid conditions. Patients' with fistulas have high mortality rates and a poor quality of life. The goal of this thesis was to develop a prototype and computational model of a minimally invasive fistula occlusion device. The prototype was designed to be an electromagnetic catheter that could deliver a glue plug to a precise location. It used a solenoid to control the magnetic field and plug delivery.

The design of the prototypes went through several stages before arriving at the final construction. Various materials were attempted for the solenoid core and a range of wire sizes for the copper coil. The final manufacturing process involves alternating coats of iron paint and iron wire for the core with a copper wire coil.

Horizontal and vertical magnetic force experiments were conducted to analyze the effects of core size. Three different sized cores were built to determine how much iron was needed to achieve a clinically relevant magnetic force. It was demonstrated that it is possible to achieve the necessary force using hollow solenoids.

A computational model was built in MATLAB so that the researchers could analyze a greater range of design parameters moving forward. Validation and verification of the model has shown magnetic field shapes consistent with solenoid theory.

The results of this study indicate that the ideas presented in the preliminary patent filed in July of 2015 are feasible. Further refinement is necessary to create the final device to be used in patients but it is possible to develop an electromagnetic catheter to control small plugs for fistula repair.

# Acknowledgements

The author wishes to express immeasurable gratitude to her many advisers, family and friends. Thank you to Dr. Wilson for allowing me to explore an avenue that is untraditional in graduate research. Thank you to Drs. Waller and Gilroy for your support through the University of Kansas Medical Center, physician assistance and innovative ideas on the end goal for this project. Thank you to Dr. Stiles for your electrical engineering expertise and assistance in calculating the equations governing the computational model; especially when fistulas are far from your area of research.

To my family, who has listened to my research for the past two years and has supported me through the good days and the bad. Thank you to my parents and brother who have traveled for my defense. A special thank you to my boyfriend, Dan, even though you are not an engineer you have helped me think outside the box and supported me. Additionally, "upstairs" deserves a special thank you for helping me bounce design ideas and for technical support when I needed a second set of hands. A special thank you to Jeremy Shui, Worcester Polytechnic Institute, for coding assistance.

This work would not have been possible without the financial support of the Madison and Lila Self Graduate Fellowship. Additional financial support for the materials involved in this research provided by the Graduate Research Fellowship at the University Of Kansas School Of Engineering.

# Contents

Abstract ..... iii

Acknowledgements ..... iv

Chapter 1: Background & Significance ..... 8

Introduction ..... 8

Background ..... 9

Current Closure Techniques ..... 12

Traditional ..... 13

Clip ..... 14

Plug ..... 15

Fibrin Glue ..... 16

Cyanoacrylates ..... 18

Ferrofluids ..... 19

Background ..... 19

Magnetic Forces ..... 20

Biomedical Applications ..... 21

Summary of Electromagnetics ..... 23

Significance ..... 24

Innovation ..... 25

Chapter 2: Design Process and Construction of a Novel Fistula Occlusion Device ..... 27

Introduction ..... 27

Qualitative Needs ..... 28
Minimally Invasive ..... 28
Hollow ..... 29
Magnetic Force ..... 29
Design Specifications/Needs ..... 30
Preliminary Results ..... 31
Iron Core ..... 32
Copper Coil ..... 33
Final Design Assessment ..... 34
Challenges ..... 37
Final Design in Detail ..... 38
Chapter 3: Early Prototypes and Analysis of a Novel Fistula Occlusion Device ..... 39
Methods ..... 39
Horizontal Experiments ..... 39
Vertical Experiments ..... 40
Results ..... 41
Horizontal Experiments ..... 41
Vertical Experiments ..... 43
Discussion ..... 45
Chapter 4: Computational Model of a Novel Fistula Occlusion Device ..... 47
Methods ..... 47

Results ..... 49

Validation and Verification ..... 49

Parametric Analysis ..... 52

Discussion ..... 53

Chapter 5: Conclusions and Future Work ..... 55

Current Limitations ..... 56

Future Work ..... 57

Conclusion ..... 59

References ..... 61

Appendix A---Math Model ..... 64

Appendix B---MATLAB CODE ..... 85

Appendix C--- Parametric Analysis Figures ..... 87

# Chapter 1: Background & Significance

## *Introduction*

The goal of this study is to propose and validate a device for repairing fistulas. Fistulas cause significant morbidity to patients, and are difficult to treat. Current treatment options are insufficient for a large population afflicted worldwide. The technology presented in the following chapters takes the failures associated with other fistula repair devices and approaches the problem from an entirely different perspective. Instead of removing tissue, we seek to plug the hole with glue. This thesis describes the steps taken so far towards developing the fundamentals of this device. Additionally, a provisional patent has been filed on the technology.

The remainder of chapter one focuses on the background information, biology and scope of the problem. In summary, there are four current closure techniques being used by physicians, each with unique advantages and disadvantages. Unfortunately, no current repair technique is successful in all situations. Surgery is successful in about 80% of patients, the highest success rate by far, but many patients are not surgical candidates. Surgery is also invasive, painful, expensive, and can cause additional fistulas. It does not come without significant risks. Ferrofluids have never been used to attempt to fistula closure, however, they are a relatively new technology that could increase the controllability of biocompatible glues. Research suggests that they may be a viable option for use in this application. Lastly, chapter one also describes the significance and innovation of the work presented in this thesis.

Chapter two covers the design process for an electromagnetic catheter and construction of the individual prototypes. Although one style of prototypes were used in the testing and evaluation

phase, descriptions of earlier prototypes that informed design decision are presented here. This chapter provides insight to the design decisions that were made as well as what type of specifications and parameters were defined in developing the device.

The third chapter describes the experimental testing of the physical prototypes. The goal is to understand the effects of different design parameters on the output of the magnetic field. It also discusses the challenges that the team faced during design implementation due to small-scale manufacturing.

Since it is impossible to build and test every prototype combination, a computational model was developed in chapter four. This chapter explains the modeling assumptions for determining the force produced by the solenoid. The computational model is important to the overall study because it can validate the phenomenon seen in chapter three. In turn, the physical prototypes also help to inform the model so that it can be used for more fine iterations.

Finally, chapter five describes the conclusions that can be drawn by taking into account the results from the physical prototypes as well as the information provided by the computational model. Additionally, future work is proposed in detail as the device is not finished. There is significant work to be continued in the development and testing of the device before it is ready for early clinical trials.

## *Background*

Fistulas are a pathological tunnel between two hollow organs within the body [1]. Figure 1A shows a generic enteric fistula tract. Figure 1B shows an enterocutaneous fistula.

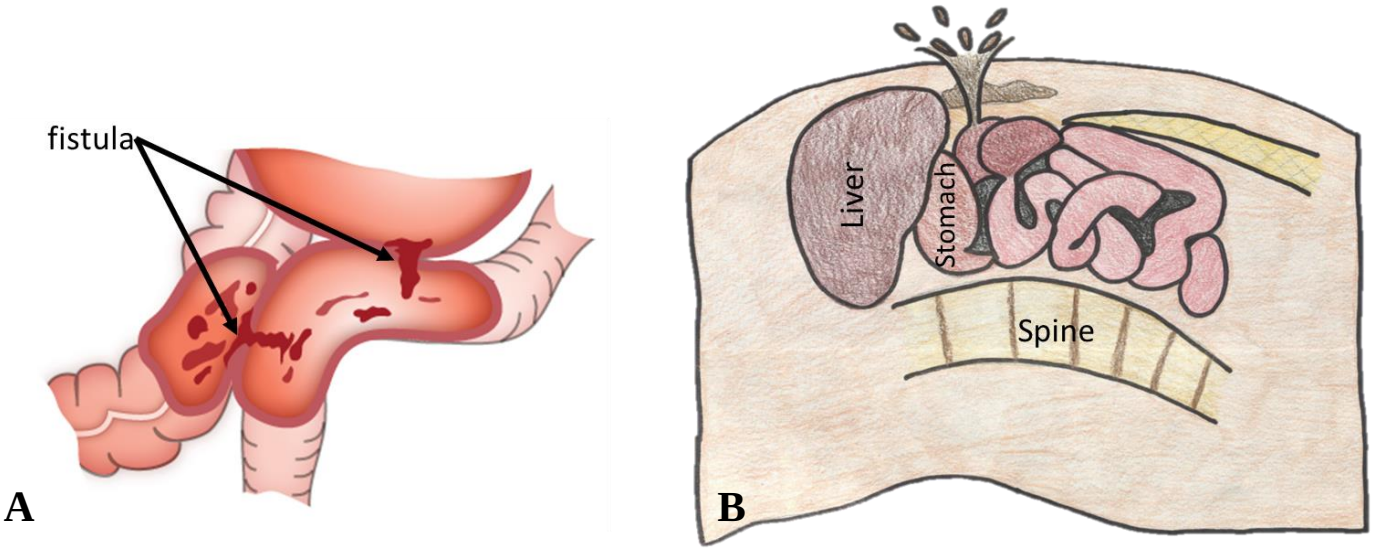


**Figure 1: A- Enterenteric and gastroenteric fistula [2] B- Enterocutaneous fistula.**

Fistulas most commonly occur between the gastrointestinal tract or biliary system and the skin or between two abdominal cavities, for instance the bowel and bladder [1]. The exact prevalence of fistulas in the US populations is unknown due to under-reporting, however the enterocutaneous pathology effects approximately 2% of all bowel surgeries (25% for open) [3,4]. Additional causes include: removal of a gastronomy tube, trauma, diverticulitis, Inflammatory Bowel Disease (IBD), and radiation therapy [5–7]. As many as 75% of enterocutaneous fistulas are thought to be iatrogenic, i.e. inadvertently caused by a physician or medical treatment [4,8].

Fistulas can be classified by either the organs that they connect, drainage levels, or tract orientation [9,10]. The anatomic naming convention has the origin organ first and the drainage organ second. For the example shown in Figure 1B, “entero” is for the intestine, and “cutaneous” is for the drainage organ, the skin. Fistulas can be classified has high, medium or low output. The higher the output the more likely the need for surgical intervention. Additionally, tracts can be simple or complex. Simple tracts are singular and have not developed abscesses or additional infections. Complex fistulas frequently involve multiple tracts, loops, other tissues and

complications. Although fistulas can occur in almost any organ system, the remainder of this thesis will focus on fistulae of gastrointestinal origin. The technology presented, however, could be later applied to biliary, urinary, and cardiovascular fistulas.

Gastrointestinal fistulas are difficult to repair and the only current method is invasive surgery that removes some of the surrounding and potentially otherwise healthy tissue [11]. Some patients are not surgical candidates because of comorbid health issues including severe malnutrition that can occur as a consequence of the fistula. In addition surgery can present a risk in some instances for loss of sphincter function and with this fecal continence can be lost [12,13]. Unfortunately, less than 25% of fistulas heal spontaneously [1,6,14].

Unrepaired fistulas can lead to significant morbidity, potential mortality, and are associated with prolonged hospitalization and costs. Sepsis may accompany gastrocutaneous fistulas with reported mortality rates as high as 85% [6,14,15]. As a function of the challenges, morbidity, potential mortality, and costs associated with fistulas the medical field continues to search for better solutions to this challenging clinical dilemma.

Mechanical closure methods include clips and plugs. Comprehensive studies on the application of clips are extremely limited and a vast majority of the available literature is reliant on individual case studies [5]. Approximately 50% of all clips fail due to poor clip position, early detachment and densely epithelialized tissue preventing adherence and inflammation surrounding the clip which contributes to foreign body reactions [5]. Plugs are the newest advancement in fistula repair. They can be made of synthetic silicones or bio absorbable xenografts which lessen the foreign body reactions. They are currently being used exclusively for anal fistulas. Despite the recent innovation, plug extrusion occurs in between 10-41% of cases and only heals 49% of fistulas in twelve months [16,17].

Additionally, various forms of glues have been explored as a non-surgical closure method with limited success; typically because of the inability to maintain a precise location once injected [18]. Before curing, cyanoacrylate has a low viscosity, which allows it to easily flow through the catheter, however this benefit is offset by the continued flow in the body and absence of precision for deployment. Decreasing the cure time of cyanoacrylate is possible with additives; however, additives often clog the injection catheter causing it to stick to the delivery site. Precision is especially important in the closure of fistulas because of possible unwanted occlusion downstream of the abdominal viscera from which the fistula originates. This particularly applies to bilioenteric fistulae.

Although new innovations have offered promise to patients, re-fistulization occurs at a rate of 11% [8]. Additionally, despite the decrease in mortality rates in recent decades, the number of patients treated non-operatively remains the same [18]. This indicates a need for a minimally invasive and greatly effective method of permanent closure of fistulas. This technology might also be applied to other areas where precise occlusion of an area is required, for instance occlusion of aneurysmal dilation of blood vessels.

A literature search for the current gastrointestinal fistula closure devices was performed using publications from the last 20 years. Papers were excluded if they focused on biological tissue grafts. Traditional techniques include various surgeries and conservative antibiotics. Other closure methods were limited to mechanical devices.

## *Current Closure Techniques*

According to a literature search there are four main categories for fistula closure: traditional, including surgery and antibiotics; clips; plugs; and fibrin glue. Although innovative,

the newer technologies have yet to show consistent results that indicate they are worth replacing the more prominent traditional methods among physicians.

## Traditional

Traditional fistula closure methods include conservative therapies like fasting the patient for extended periods of time and placing them on total parenteral nutrition (TPN), antibiotics and octreotide. In addition, should this fail, the less appealing, surgical intervention option might be considered. Most physicians agree that a conservative approach makes sense during initial treatment, however, less than approximately one-third of patients will respond to this resulting in spontaneous closure of their fistula [6,18]. Octreotide can decrease the output of the fistula by 50% in those patients who respond by reducing gastrointestinal secretions, motility, and enzymatic activity [19]. Octreotide, however, has potential side effects. In general a combination therapy of medications including octreotide and antibiotics coupled to TPN is widely used with variable success [15].

Unfortunately, more than two-thirds of patients have high output fistulas or do not respond to these more conservative measures [6,18]. For those failing the conservative approach, surgery is ultimately required if not contraindicated. Operations are successful in more than 80% of patients, but are expensive in time, money, and carry significant morbidity including pain [8,18]. There are a few surgical techniques used: re-anastomosis with a limited resection, endoscopic suturing and mucosal de-epithelization, and covering the fistula with a skin graft [7,20]. As previously stated, many patients demonstrating a gastrocutaneous fistula are not surgical candidates because of their age, comorbidities or health status, and are therefore limited in their treatment options.

## Clip

Over the-scope clips (OTSC) were designed for closure of intestinal perforations, fistulas and leaks. As shown in Figure 2, the clip is deployed through the scope by the physician under visualization.

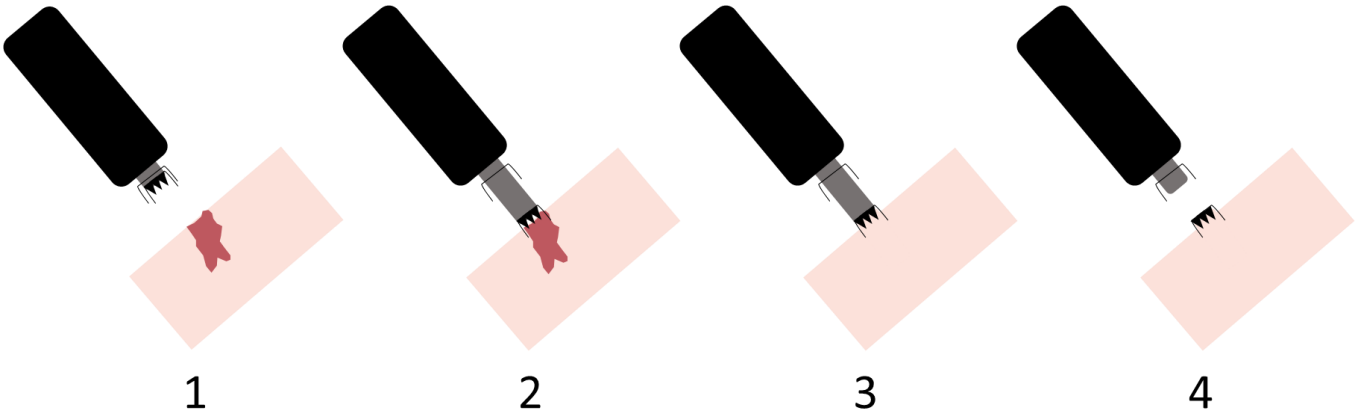


**Figure 2: OTSC deployment. Step 1 shows the scope coming into visualization of the affected tissue, step 2 is the initial attachment of the clip to the tissue, step 3 is closing of the fistula by pulling healthy tissue together inside of the clip, and step 4 is the removal of the scope leaving the clip in place.**

The scope is inserted through the rectum or the mouth depending on the location of the fistula. In the case of small bowel fistulas the endoscopic approach may not be possible as the endoscopic equipment has limited length and maneuverability. Once the affected area is visualized, the clip attaches to the healthy tissue and pulls it together covering the pathological area. This provides opposition of surfaces to close the fistulous tract and to allow an opportunity for the tissue to heal itself. The clip falls into the lumen of the intestine with time and hopefully during the period of tissue opposition the natural process of wound healing leads to closure of the tract by fibrotic mechanisms and healing of the intestinal mucosa by regrowth over the defect.

The ability to deploy clips successfully is highly variable and ranges from 38-100% [21]. Long-term results of this technique are not well studied, with concerning estimations of a 50%

recurrence rate despite technical success of clip deployment and initial closure of the internal defect [21]. Clip failures occur for several reasons: poor clip placement by the doctor, early detachment from the tissue and densely epithelialized tissue [5]. Because of these early and long-term failures, clips are considered an additional part of combination therapy but should not be used universally for fistula closure [10].

### Plug

Plugs are the newest technology to enter the fistula space. Currently they are exclusively used for anal fistulas, but are being explored for other avenues. There are two commercial plugs described in the literature, one known as the Cook Biodesign plug made of a xenograft and the other, Gore Bio-A made of synthetic material. Unfortunately, few long-term studies exist in order to quantify the potential success of these plugs. The hypothetical insertion of the plug can be seen in Figure 3 [2].

The Biodesign Anal Fistula Plug (AFP) is made of a bio absorbable xenograft from lyophilized submucosa of porcine small intestine [22]. Adamina et, al. performed a cost analysis and although 50% of the fistulas closed, they were unable to draw conclusions regarding comparison to traditional surgical techniques. However, AFP did cost less than traditional therapy it was likely due mostly to the decreased length of the hospital stay [22].

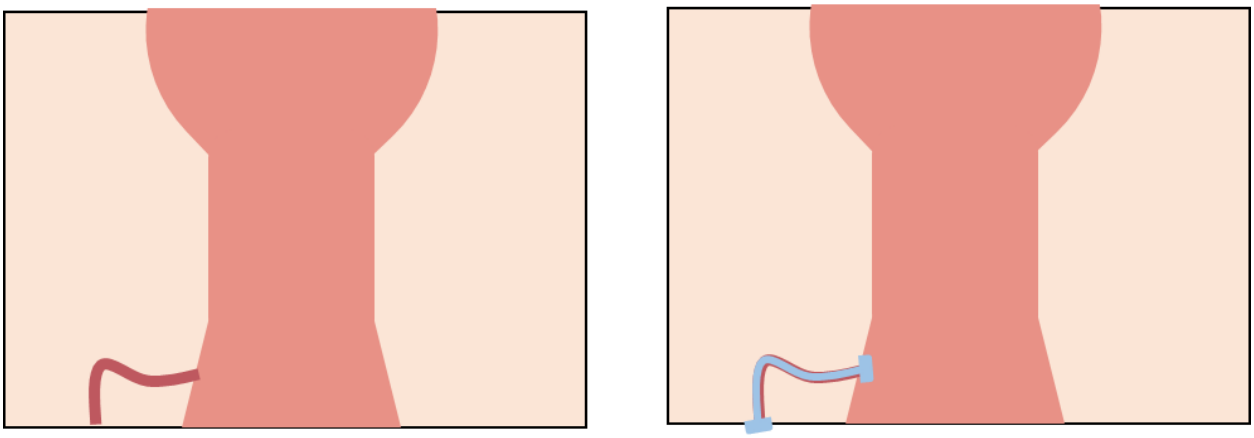

**Figure 3: Anal fistula and deployment of Anal Fistula Plug (AFP).**

The Bio-A plug is made of a composite of polyglycolic acid and trimethylene carbonate (PGA:TMC) tubes and absorbs between seven and ten months [17]. It was implanted in an outpatient setting. At twelve months about 49% of patients had healed completely [17].

Failures from AFPs are typically caused by a mismatch in plug to fistula tract width resulting in plug extrusion. This occurs in 10-41% of patients [16]. Additionally, many patients demonstrate contraindications that make them ineligible for an AFP including: vaginal involvement, persistent abscess, infection, allergy to porcine products, and inability of the physician to identify openings [16]. Although the success rates are not nearly as high as the medical community would like, AFPs are known to have lower complication rates than alternative surgical methods. This indicates a place for them in treating complex anal fistulas [23].

## Fibrin Glue

Although the concept of using fibrin glue in medical applications has been around for many decades, it has not been widely used [24]. Consequently, few studies have been performed to analyze its highly variable (14-60%) success rate [25]. Instead, case studies are available regarding its effectiveness. Fibrin glue is usually used in patients that are not surgical candidates indicating a bias in the patient population for the case studies.

Shand et al, describes a patient who was identified as high surgical risk after she pulled out her PEG tube forming a gastrocutaneous fistula [24]. The patient was started on TPN and octreotide, traditional conservative fistula treatment methods. Foley catheters were introduced to drain the fistula but once the fistula size was reduced to 14 French, high output of gastric juices continued, and smaller catheters were unable to provide adequate closure. Since the patient was a high risk for surgery, the team at Western General Hospital in Edinburgh initiated an endoscope to deploy Surgicel, human fibrinogen and human thrombin. Additional components were injected directly through the abdominal wound. Complete closure of the mature fistula tract was achieved in 11 days [24]. This case study in 1997 was foundational for the investigation of the use of fibrin glue in future fistula closures.

Additional case studies indicate similar results using the same technique [14]. However, multiple endoscopic sessions were often used and the sample size has been extremely limited. Fibrin glue seems to be a promising alternative to surgical management, however more significant results are needed before any conclusions can be drawn.

Although gastrocutaneous fistulas are an uncommon complication, they can be debilitating towards the patients with whom they affect. Coupled with ineffective treatments and poor success outcomes can cause significant morbidity. Although the mortality rate has decreased in recent years from 43% in 1960 to 7% in 2006, the number of patients being treated non-operatively remains the same [18]. Fistulas are complicated and re-present in as many as 63% of patients even months after the initial fistula was thought to have healed [25]. This provides an attractive opportunity for technological advancement. Clips, plugs and fibrin glue are less invasive methods, but their success rates dwarf that of traditional fistulotomy.

The studies presented here are limited by their small sample sizes. Unfortunately fistulas often present with comorbidities which makes patients ineligible for treatment. Additionally, a small portion of the general population will present with a fistula and an even smaller portion will adhere to a clinical trial [17]. Randomized control trials with long-term clinical follow up are needed in order to accurately determine success rates of each technology [22].

The community is yearning for an option better than the current state of technology described. Each method has qualities that make it attractive for further investigation, however, without reliable and consistent results it is difficult for researchers to determine which technology presents the most promise.

## *Cyanoacrylates*

Cyanoacrylates are a class of adhesive monomers that polymerize into chains when exposed to moisture. Originally developed in 1942, cyanoacrylates have been used extensively for commercial use since the 1970's. During the late 1960's, cyanoacrylates were tested on the battlefield to assist in the control of bleeding in soldiers. Nevertheless, FDA approval for medical uses did not come until much later due to irritation. Later, the FDA approved the use of 2-octyl cyanoacrylate (Dermabond) in closing wounds and surgical incisions. Interventional radiologists have also used cyanoacrylates to treat vascular malformations and aneurysms. They have been used limitedly to seal biliary leaks and enteric fistulas. Success rates are varied since there are such limited case studies.

Several varieties are available as medical grade and have been used most commonly to close surgical wounds but have also seen success in aneurysms and occluding tissue varices [26]. The main complication with using cyanoacrylates in the body is maintaining precise control of the location of the adhesive. Before curing, the cyanoacrylate has a low viscosity, which allows it to

easily flow through the catheter, but then continues to flow in the body. Decreasing the cure time is possible with additives; however, then it often clogs the injection catheter causing it to stick to the delivery site. Precision is especially important in the closure of fistulas as inadvertent occlusion of vessels downstream can lead to a worse outcome than no intervention. Thus increasing the controllability of cyanoacrylates is a desirable feature for its application in closing fistulas.

## *Ferrofluids*

### Background

Ferrofluids have been a topic of interest for the past few decades. Their applications are vast and include: microfluidics, actuators, and stepper motors just to name a few [27,28]. Ferrofluids are stable suspensions of ferrous nanoparticles in a carrier liquid, either oil or water [27–30]. The particles are coated with a surfactant which prevents aggregation, even in the presence of intense magnetic fields. Because of their size, Brownian motion keeps the particles from aligning in the fluid and allows the ferrofluid to behave as a paramagnetic material [29,30]. That is, it only maintains a magnetic moment when exposed to the magnetic field.

This phenomenon is useful because it potentially can allow for control over the movement of the fluid through indirect contact: magnetic field presence. The field of ferrohydrodynamics embraces the complicated nature of ferrofluids and hopes to understand the mechanics of motion as influenced by magnetic polarization [29]. Ferrohydrodynamics includes the study of all ferrofluids, however, there is significant literature demonstrating just how vast that field is. Ferrofluids can have a variety of: sizes of nanoparticles, surfactants, and carrier fluids. Most interesting to medical applications are ferrofluids suspended in water because they are potentially biocompatible.

Several companies market ferrofluid compounds for purchase, including FerroTec, the only retailer of biocompatible ferrofluid (disclaimer: not FDA approved) [27]. The existence of these companies shows that there is value to creating technologies using ferrofluids.

## Magnetic Forces

With the absence of a magnetic field, the nanoparticles are randomly oriented in the fluid and the rheological properties are most similar to that of the carrier liquid [31,32]. In the presence of a magnetic field, however, the nanoparticles of a ferrofluid orient themselves according to field lines [28]. This re-orientation phenomenon has multiple effects on the behavior of the ferrofluid. The change from Newtonian to non-Newtonian behavior is what makes them interesting for applications [33].

For dilute ferrofluids, magnetic inter-particle interaction is negligible [34]. However, when a magnetic field is applied, strong inter-particle interactions take place, especially in fluids composed of nanodiscs [31]. These inter-particle interactions, or magnetoviscous effect, are what are responsible for the shape changes in ferrofluid droplets [30,35]. According to Rahmani, in the presence of magnetic fields, ferrofluids stretch out perpendicular to the field source based on their constrained geometry [29]. This is true even in complex containers beyond the capillary tube. Additionally, they concluded that blob shape can influence its behavior within the container. This finding is useful in developing technologies that involve detaching from walls [29].

When designing devices that use ferrofluids, it is interesting to note the rheological changes that occur in the presence of a magnetic field. It seems obvious that as a field is applied the viscosity increases. However, Borin et al found that the viscosity increases up to 40 times that of the fluid without a magnetic field [31,32]. This is an extremely important result as it alters the

behavior of the fluid so significantly geometries and force applications must be different depending on if a field is being applied.

Previous research has been conducted on magnetic flux density and the force applied to ferrofluid blobs [36,37]. Both analyses are important when determining characteristics of potential devices utilizing ferrofluid technologies. Mefford et al calculated the force on a droplet of ferrofluid from both permanent and electromagnets. For low currents, the theory matched the experimental results. However, at high currents (3A or greater), it over-predicted the force [37]. This is especially important in the use of electromagnets for ferrofluid applications.

## Biomedical Applications

There are three studies that have greatly influenced the use of ferrofluids in biomedical applications. Each are early experiments but have been foundational in the development of prototypes. Thiele et al, used ferrofluids to control the manipulation of hyperbaric lidocaine in spinal anesthesia [38]. Paschalis et al, designed an implantable glaucoma valve for the eyeball using ferrofluid [39]. Mefford et al, analyzed the movement of a ferrofluid blob through the vitreous humor towards an external magnet for retinal detachment repair [37]. Although unrelated in application to the research presented in the subsequent chapters, the findings of each were critical to the innovation of the prototype design.

Cardiac arrest is a serious and life threatening complication potentially arising from spinal antiesthetic. Gravity causes hyperbaric drugs to move in the spinal column; reaching T-4 can be detrimental to the patient. Currently, anesthesiologists influence block height by adjusting the patient's back position in relation to the ground. Thiele et al, wanted to use ferrofluids to influence nerve block height against gravity [38]. In the pilot study they used PVC tubing to create a model of the spine and inject it with a magnetic methylene blue-lidocaine solution and a non-magnetic

solution. The external magnet had no effect on the non-magnetic solution whereas it completely prevented gravitational dependent settling in the magnetic solution. This is promising for using magnetic fields to control the placement of other fluids through mixtures. There was no evidence of separation of the fluids, indicating the ferrofluid actually "pulls" other fluids along if mixed well [38].

Glaucoma causes blindness due to increasing intraocular pressure (IOP). Many devices and pharmaceuticals exist aiming to reduce IOP [39]. However, most of these valves rely on the encapsulation process of the plate. Paschalis et al set out to design a valved tube capable of regulating IOP without relying on encapsulation [39]. In this instance, Ferrotec's ferrofluid was injected to a small capillary tube. Two micro magnets securely fixed the ferrofluid in place and acted as the pressure regulator. The valve worked according to the changing-shape phenomenon previously described by Rahmani and seen in action here [29,39].

Retinal detachment is another leading cause of blindness. Current treatments fail often and effect millions worldwide. Mefford et al developed a biocompatible ferrofluid to repair retinal tears [37]. The fluid is injected into the vitreous cavity and a permanent magnet is placed underneath Tenon's capsule. The magnet attracts the ferrofluid droplet across the vitreous humor and seals the hole. Their research used theoretical calculations and experimental results to validate their proposed therapy. Assuming steady-state velocity, the team calculated the magnetic force for every distance point from the magnet. This same principle will be applied in calculations seen in chapter 3.

Although ferrofluids have never been used to seal enterocutaneous fistulas, these other biomedical applications demonstrate similar behaviors that are desired by this novel fistula occlusion device. Ferrofluids can be used in combination solutions with other fluids to drive

motion in the presence of a magnetic field [37,38]. Additionally, they are expected to have good biocompatibility as required by the FDA [39]. Current fistula closure techniques are insufficient, the properties and behaviors of ferrofluids make them a promising alternative.

## *Summary of Electromagnetics*

A solenoid is a coil of wire wrapped around a core, typically iron, that produces a reasonably uniform magnetic field when current is passed through the wire [40,41]. Figure 4 shows the coil of wire perpendicular to the page and the resulting magnetic field lines.

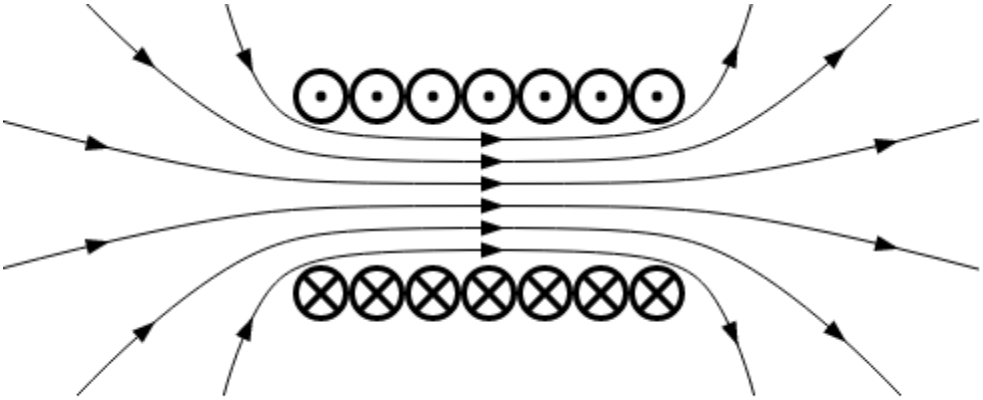

**Figure 4: Diagram of magnetic field lines in a solenoid coil [42]**

The magnetic field follows the direction of the "right hand rule"; if the right hand is placed around the solenoid with the fingers pointing in the direction of flow, in this case, out of the page, the thumb points in the direction of the magnetic field [42].

For an infinitely long solenoid, the magnetic field only occurs inside the solenoid [43]. The field inside the solenoid is given by the equation, $B = \mu_0 nI$ . Outside, **B** is equal to zero [44]. This is fine in theory, but in practice, it is important to know the field of a short solenoid [44]. For points far from the end of the solenoid, the magnetic flux density can be predicted by equation 1.1 [45].

(1.1) $$\boldsymbol{B}\ \bar{r}\ = \frac{\mu_0}{4\pi}\iint_S \frac{\boldsymbol{J}_s\ \vec{r}\ \times\ \bar{r} - \vec{r}}{\left|\bar{r} - \vec{r}\right|^3} ds'$$

This equation will be used to define the model described in detail in chapter 4.

## *Significance*

Surgical and disease complications such as fistulas can cause extreme pain to the patient as well as exorbitant medical costs. Fistulas are abnormal tunnels between two tissues within the body. These pathogenic ducts can cause serious ramifications if left untreated and current options are insufficient. They commonly occur in the gastrointestinal tract as well as biliary conduits, however, they are also seen in the vascular system. Various forms of glues have been explored as a non-surgical closure method with limited success typically because of the inability to maintain a precise location once injected. If the controllability issue could be addressed, glues have significant potential for fistula closure.

The prevalence of fistulas in the US populations is far reaching due to its various forms. If left untreated, fistulas can cause abscesses, infections and other complications. Some fistulas repair themselves or with the help of antibiotics, however, up to two-thirds require surgical intervention. Often times, these patients are not suitable to undergo additional surgeries as typically they have multiple diagnoses and are already in poor health. Therefore, a non-surgical method of fistula repair is desired. The excellent adhesive qualities make cyanoacrylates an ideal candidate to occlude fistulas. However, the inability to control its precise location leaves room for innovation. The device proposed in this document will make fistula repair non-invasive and contribute greatly to the quality of life of many individuals.

### *Innovation*

The need for a non-surgical, simple method of repairing fistulas has been made evident. However, the precision needed to control potential non-invasive treatments does not currently exist. The proposed device looks to mix cyanoacrylate with a biocompatible ferrofluid in order to control with exacting precision the location of the cyanoacrylate until it forms a solid plug.

Previously, magnetic particles have been used previously to safely retract the bowel during other surgeries [46]. In the given case study, the particles are flushed from the system once the external magnets are removed. Biologically compatible ferrofluid has also been used in experimental procedures mixed with lidocaine for spinal blocks [38]. This provides novelty because there is currently no mechanism to control cyanoacrylate inside the body. Utilizing the inherent properties of ferrofluids will allow the cyanoacrylate-ferrofluid plug to act as a permanent solution for fistulas.

The proposed device is innovative in its approach to precisely placing the cyanoacrylate-ferrofluid adhesive plug. The delivery catheter will contain a solenoid at the distal end. When power is turned on, the solenoid will produce a magnetic field and influence the ferrofluid-glue solution. This magnetic field will maintain the location and will prevent the plug from adhering to undesired areas, such as adjacent ducts and vascular structures. The result is a permanent, obstructive, intact tissue-adhesive plug.

A minimally invasive procedure is novel in the field of fistulas. Currently, fistula treatment requires extensive surgery under general anesthesia and several weeks of recuperation following the procedure. This typically is associated with hefty hospital costs and is painful for the patient. The device proposed is intended to be used with a catheter, resulting in less pain to the patient, a

shorter recovery period and lower overall costs. The procedure will also provide a permanent fix, with no need for secondary procedures.

The focus of this thesis is to develop the electromagnetic catheter component of the glue delivery system. Many designs were taken into consideration and one type prevailed for further analysis. The variations in that type of prototype were tested for magnetic field strength that would be clinically applicable. Additionally, a computational model was constructed to provide further insight and allow for refinement in the design moving forward. Together the results of the physical prototype and the computational model inform the future work of this product.

# Chapter 2: Design Process and Construction of a Novel Fistula Occlusion Device

## *Introduction*

Fistulas are difficult to repair and the only current method is invasive surgery that removes some of the surrounding and potentially otherwise healthy tissue [14]. Some patients are not surgical candidates because of other health complications [12]. Various forms of glues have been explored as a non-surgical closure method with limited success, typically because of the inability to maintain a precise location once injected. Before curing, the cyanoacrylate has a low viscosity, which allows it to easily flow through the catheter, but then continues to flow in the body. Decreasing the cure time is possible with additives; however, they often clog the injection catheter causing it to stick to the delivery site. Precision is especially important in the closure of fistulas because of possible vessel occlusion downstream.

If the location control issue can be addressed, cyanoacrylates are a promising method of fistula closure that can be delivered non-surgically. Ferrofluids are an innovative solution to the delivery precision problem. Ferrofluids are iron particles suspended in either oil or water based solutions that react to the presence of a magnetic field.

The goal of this project was to develop a system that could deploy magnetic glue and control its position using the magnetic field from a solenoid. This chapter describes the iterative process of early prototype development as well as the final manufacturing protocol for the devices. The final prototypes are evaluated in chapter 3.

## *Qualitative Needs*

The idea for this device was developed out of the Internal Medicine Department at the University of Kansas Medical Center. Drs. Richard Gilroy, Philip Johnson and Stephen Waller approached the University of Kansas's College of Engineering with their problem and proposed solution. They had experimented with controlling off-the-shelf ferrofluids with external magnets. However, designing a medical device is not that simple. The device needed to be: minimally invasive, hollow in order to inject fluid into the body, and hold a bolus of fluid in place for the duration of the curing time. Additionally, all medical devices must meet strict guidelines provided by the FDA complete with rigorous benchtop and clinical testing. In the early stages these guidelines were kept in mind in regards to design decisions but they were not the specific goals of the project.

### Minimally Invasive

The current gold standard for fistula repair is an invasive surgery. Unfortunately, many fistula patients are not surgical candidates due to comorbidities or their current state of health. This leaves them susceptible to abscesses, infections, sepsis and even death. Antibiotics are frequently prescribed, however, less than one-third of patients respond [6,18]. This gap in care is the motivation behind the development of the fistula occlusion device. A better method of treatment must exist for these patients.

Additionally, those who are able to withstand a surgery are faced with the risk of severe complications, including recurrent fistulas. Surgery is successful in about 80% of patients but does not come without the downsides of cost and pain [8,18]. A device that can repair a fistula using

interventional radiology techniques is highly desirable and would disrupt the healthcare model used today.

"Minimally invasive" is indicative of the small size of this device. In order for the device to be used non-surgically, it must fit through ducts the body already has, such as the biliary tract or gastrointestinal system.

### Hollow

Not only does the catheter need to produce a magnetic field, but it must be hollow so that magnetic glue can be deployed through its lumen to the desired site. This seems obvious, however, little research has been performed on the effectiveness of magnetic fields from a hollow solenoid. Most solenoids that are a commercially available or those used for similar applications have a solid core of a highly permeable material.

### Magnetic Force

Lastly, but most importantly, the device must produce a magnetic force strong enough to hold a bolus of ferromagnetic glue in place while it cures. Presence of a magnetic field is suggestive of magnetic force, but they are not explicitly related [28]. Solenoids can be used to create an electromagnet which, when powered, can produce a magnetic force [47]. Solenoids were chosen because they are capable of turning on and off [28]. Although previous research indicates a method for controlling the profile of solenoid magnets, this is much easier in simulation than in practice [48,49].

## *Design Specifications/Needs*

These qualitative descriptions of what functions and features the fistula occlusion device needed to have were nuanced into the three main design specifications presented in Table 1. The diameters were determined explicitly through catheter measurement of what is commercially available. In order for the device to be minimally invasive it must use a catheter based foundation. Because of the size of vessels, the device is strictly limited to these physical dimensions. Additionally, the 0.52 g of weight the device needs to be capable of holding is what is relevant for this application. This was determined from physician consultation and approximation using characteristics of a commercially available glue, Trufill n-BCA [50] . Should the application change, or the formulation of the glue change, the force will need to be re-evaluated. The weight is representative of the amount of glue the catheter would need to deliver to be useful to the physicians as a repair tool. Future work will involve more exploration of this specification to understand its adequacy. Anything less than this value, however, is seemingly useless.

**Table 1: Design specifications as determined from the qualitative needs of the device.**

| **Parameter** | **Value or Range** | **Unit** |
|---|---|---|
| Inner diameter | 0.97 | mm |
| Outer maximum diameter | 1.5-4.0 | mm |
| Weight to be held | ≥0.52 | g |

The other engineering specifications of the device were not outlined prior to the design process as they have more flexibility. For the first generation of the prototype, the technology was built on a commercially available catheters. However, future iterations may choose to re-design the catheter scaffold which would change these design specifications.

## *Preliminary Results*

The goal of this research was to develop a device to control a magnetic glue plug in the body. A schematic of the general idea is presented in Figure 5.

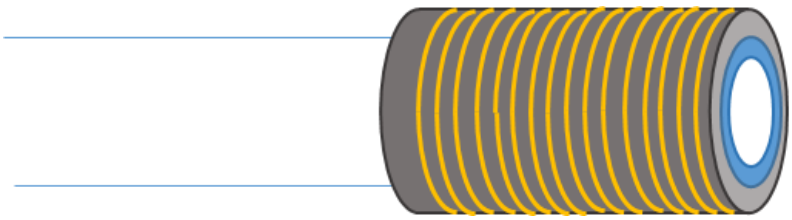

**Figure 5: General schematic of what the device should look like; blue is the internal catheter, grey is some type of iron or metallic core and gold is a solenoid coil. This generic setup was used to guide the future designs.**

Many iterations of the prototype were attempted before arriving at the final design. Sizes for the copper coil and materials for the iron core were optimized both for manufacturing and magnetic force. As shown in equation 1.2, the magnetic field is determined by three design parameters.

(2.1) $$B = \mu \times \frac{n}{l} \times I$$

The permeability, μ, is most strongly correlated to the material property. Iron is significantly more permeable than most other available materials like zinc or cobalt, however some advanced ceramics exist that could be explored in the future. The amount, or weight of iron in the core influences the total permeability so that was examined when building potential cores. Turns per unit length, or *n/l*, is also highly influential. The gauge of the copper coil determines the turns per length. Current, is the most accessible since it can be evaluated on every prototype simply by altering the power supply.

## Iron Core

Several materials were explored for use in the iron core. Small metal tubes are commercially available, however, they are typically made of zinc or steel instead of pure iron to decrease the opportunity for oxidation to occur. They also tend to have larger lumen than necessary for the application with thinner walls. The permeability difference between steel and iron is greater than three orders of magnitude. This large difference in permeability caused a significant change in the behavior of the prototypes and is considered to be the term of greatest influence. Simply changing the material can impact the overall magnetic field strength by 1000X [48].

The team also investigated the use of metal tape commonly used for mounting posters. Due to patent protection, the exact composition of the tape is unknown, however it was deemed irrelevant because of the difficulty in use for this design construction. The tape only came in one thickness which severely limited the rolling capabilities and the inner lumen could not be built as small as dictated by the design specifications.

Pure iron wire (0.35 mm) was the closest to creating unique tubes of the exact dimensions desired, however, there were obvious gaps between the coils to create the core. This finding facilitated the idea to use paint to fill in the gaps. Finally iron paint was investigated. This material was also protected by intellectual property, however, it was reported that 49.97% of the Modern Metals Iron Oxidizing Paint was pure iron while the remaining 50.03% was unknown additives [51]. Combining the iron wire with iron point was the closest the core came to being pure iron with permeability of approximately 5,000 $N/A^2$ using available materials.

During this experimental design process, it was determined that permeability had the greatest overall effect on the magnetic field.

## Copper Coil

The copper coil was investigated despite having a lesser effect on the overall magnetic field because the results of the iron core were determined simultaneously. It has a direct relationship to the overall magnetic field strength a solenoid is capable of producing. In early iterations, two types of copper wire were examined in order to predict their influence over the magnetic field. The thick wire was 0.66 mm in diameter while the thin wire was 0.33 mm. Equation 1.3 describes the relationship between the resistance in the coil and the number of turns per unit length and radius of the coil.

(2.2) $$R = \frac{l}{\pi r^2 \sigma}$$

If the radius, *r*, doubles, the amount of current the coil can withstand increases by a power of 4 whereas the number of turns only decreases by half. This lead to the hypothesis that the thicker wire would produce a stronger solenoid and thus be more appropriate for use in the final design.

An experiment was created to test that hypothesis where the core conditions were kept the same and only the type of copper coil changed between prototypes. Identical zinc spacers were used as the cores. One prototype was constructed with thicker copper wire (0.66 mm) and one with thin wire (0.33mm). The length of the coils was kept constant at 2 cm, however the thickness of the wire meant that the thick coil had half as many turns per unit length as the thin coil.

The solenoids were powered with approximately 2.5 A of current and held near steel balls vertically. An attempt was made to pick up as many steel balls as possible using the prototype. Due to gravity, the weight of the balls corresponded roughly to the magnetic force the solenoid was producing. The hypothesis was rejected because the prototypes that utilized thinner coils but more turns actually prevailed in holding more weight. This is likely due to the thickness of the

coating. Thinner wires are able to have a much greater ratio of copper to coating whereas the thicker wire had a thicker plastic coating to prevent excessive heat transmission. This finding led to using the thinner wire for all future iterations.

### *Final Design Assessment*

After analyzing many different design combinations, a final configuration was determined and built for testing. Prototypes were built on 20 cm of the distal end of Angiodynamics Soft-Vu Berenstein 5F catheters. This would allow for the eventual deployment of the magnetic glue through the 0.97 mm lumen. The solenoid was built on the last 2 cm of the catheter. To create the core of the solenoid, alternating layers of iron paint (Modern Metals Metalic Oxidizing Iron Paint, 49.97% wt) and iron wire (0.35mm) were applied as shown in steps 2-3 of Figure 6.

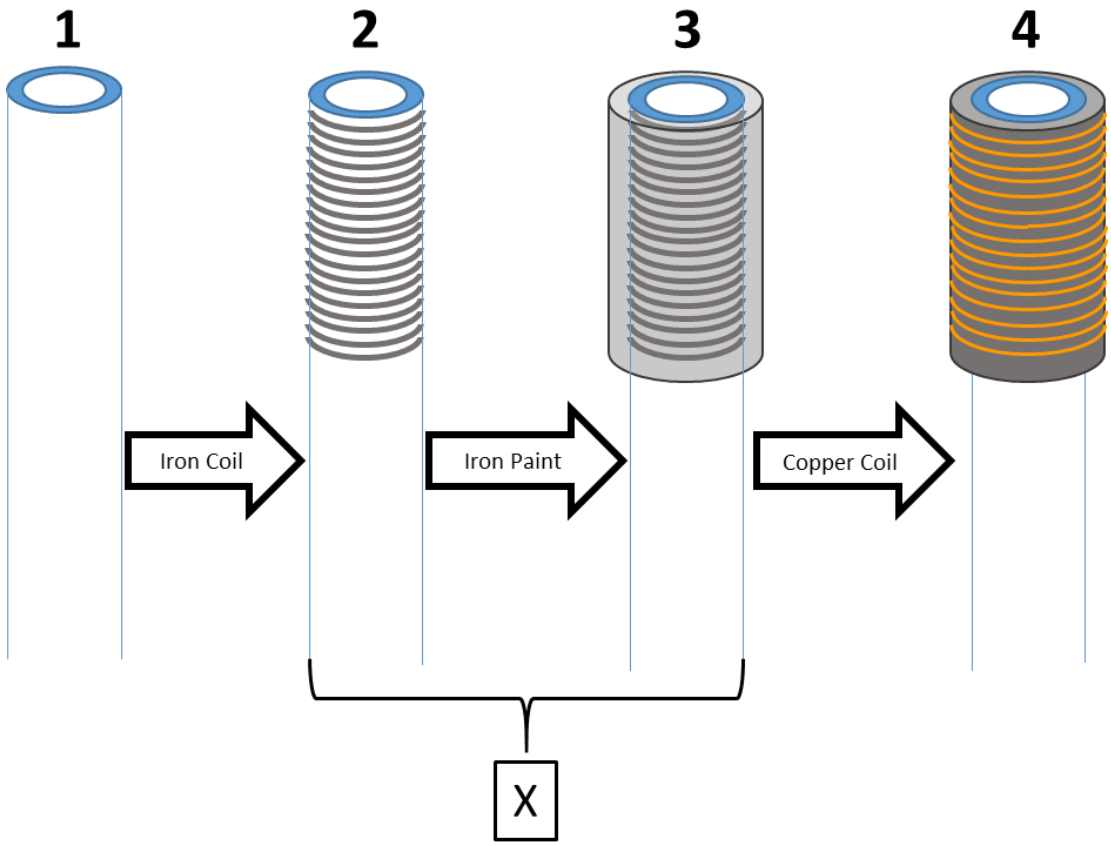


**Figure 6: Manufacturing process for creating the iron core and external solenoid on the catheter. X=2, 4, or 6 depending on which level of prototype was being built. Three of each group were created to analyze effects between similar prototypes.**

Three prototypes of each experimental group were built according to the specifications shown in Table 2. Group 2 indicates two alternating coats of iron wire and iron paint were used for the core. Group 3 indicates four alternating coats of iron wire and iron paint were used for the core. Group 4 indicates six alternating coats of iron wire and iron paint were used for the core. A, B, or C indicates the version number of that group. Three versions of each experimental group were built in order to analyze differences between and among prototypes. These materials were chosen from previous prototype iterations as described in the previous section. Weights were taken during the manufacturing process to determine similarity between prototypes of the same number and differences between different group numbers.

**Table 2: Specifications of core materials and weight for each prototype. Coat number and material in the left column indicate the step in the manufacturing process depicted in Figure 6 at which the weight was taken. For instance: 3 paint means the weight of the prototype after alternating 3 coats of wire and 3 coats of paint were applied to the core.**

| | Relative Weight (g) | | | | | | | | |
|---|---|---|---|---|---|---|---|---|---|
| **Prototype** | **2A** | **2B** | **2C** | **3A** | **3B** | **3C** | **4A** | **4B** | **4C** |
| **Catheter weight** | 0.33 | 0.35 | 0.37 | 0.28 | 0.36 | 0.35 | 0.34 | 0.35 | 0.45 |
| **1 wire** | 0.25 | 0.24 | 0.25 | 0.30 | 0.26 | 0.22 | 0.22 | 0.23 | 0.23 |
| **1 paint** | 0.02 | 0.02 | 0.02 | 0.02 | 0.03 | 0.04 | 0.04 | 0.02 | 0.03 |
| **2 wire** | 0.30 | 0.29 | 0.30 | 0.31 | 0.29 | 0.31 | 0.30 | 0.29 | 0.31 |
| **2 paint** | 0.08 | 0.09 | 0.06 | 0.09 | 0.01 | 0.08 | 0.08 | 0.05 | 0.06 |
| **3 wire** | | | | 0.30 | 0.38 | 0.35 | 0.39 | 0.35 | 0.37 |
| **3 paint** | | | | 0.13 | 0.10 | 0.17 | 0.13 | 0.05 | 0.11 |
| **4 wire** | | | | 0.43 | 0.42 | 0.09 | 0.46 | 0.40 | 0.47 |
| **4 paint** | | | | 0.18 | 0.17 | 0.54 | 0.27 | 0.18 | 0.21 |
| **5 wire** | | | | | | | 0.63 | 0.48 | 0.59 |
| **5 paint** | | | | | | | 0.41 | 0.36 | 0.38 |
| **6 wire** | | | | | | | 0.76 | 0.77 | 0.90 |
| **6 paint** | | | | | | | 0.37 | 0.72 | 0.40 |
| | | | | | | | | | |
| **Iron Core Weight** | 0.60 | 0.59 | 0.59 | 1.55 | 1.51 | 1.39 | 3.40 | 3.20 | 3.46 |
| | | | | | | | | | |
| **Avg** | 0.59 | | | 1.48 | | | 3.35 | | |
| **Stdev** | 0.00 | | | 0.08 | | | 0.14 | | |

After drying, an external coil was constructed using coated copper wire with a diameter of 0.33 mm wrapped tightly approximately 35 times around the iron core. This coil was connected to the power supply in order to create the magnetic field. These prototypes were evaluated and the results are provided in chapter 3.

### *Challenges*

There were two great challenges in developing this device. The first was communicating needs between the clinic and the laboratory. The second, was finding available materials for creating prototypes.

Physician-engineer interaction is something that is critically important to the innovation of new medical devices. However, this important aspect is not met without challenges. It is often difficult to create something tangible that meets the imagination of the end user. Engineering design is an iterative process that requires frequent refinement as testing and evaluation occurs. In this device, the communication was critical to understand the overall function of the device and the design requirements as they pertain to a non-surgical intervention. Experimental testing was originally conducted to move a steel ball, thus demonstrating an effective magnetic field strength. However, after further conversation it was later determined that the glue does not need to be moved by the solenoid per se, but instead it just needs to be held in place. This is a fundamental finding because it is obviously much easier to keep something from moving than it is to initiate motion. This greatly influenced the experimental setup seen in later chapters.

In the academic setting it is especially important to be conscious of financial resources. This often means being creative when initiating designs. Additionally, when manipulating many different design parameters it is much easier to use commercially available products to implement into the design. This was difficult because the exact material was unavailable. Ideally, solid iron tubes would have been used for the prototype but these weren't available commercially. In future iterations, this need will be addressed and compared to the results seen in these prototypes.

### *Final Design in Detail*

Three final prototypes were built and tested in subsequent chapters. Figure 7 shows the measurements of these final prototypes.

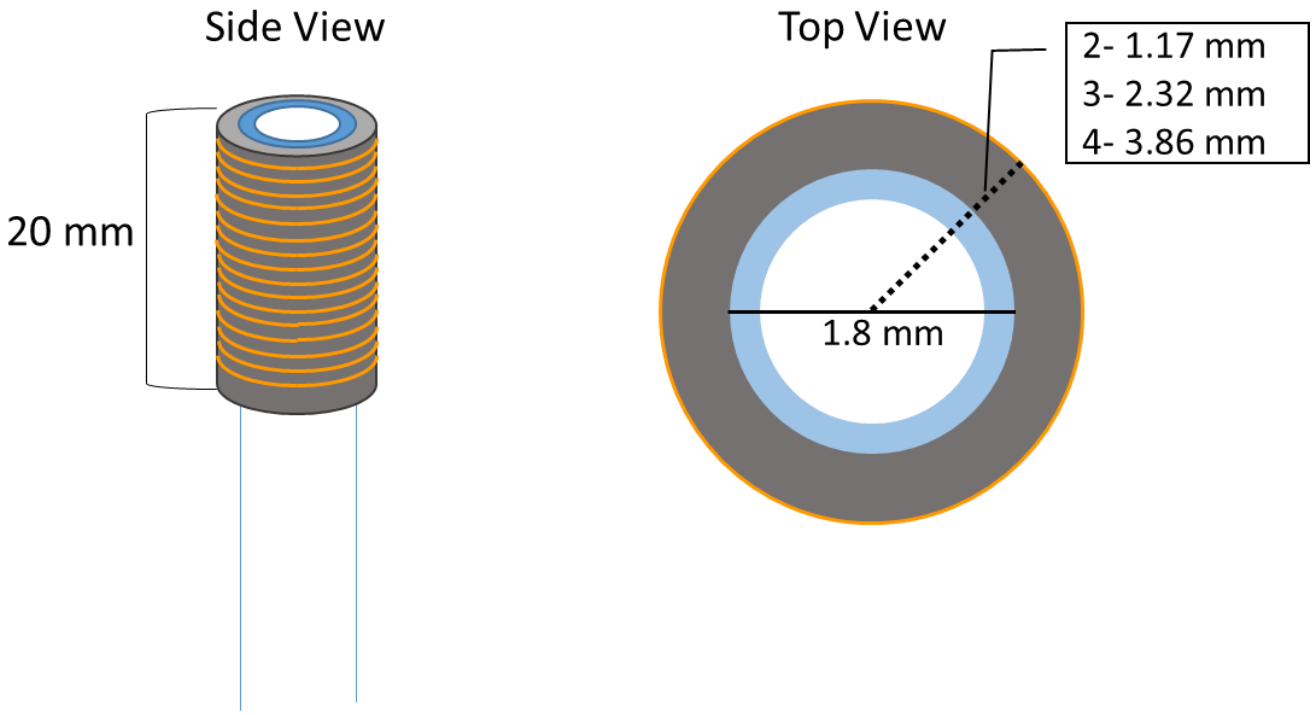


**Figure 7: Final design of the novel fistula occlusion device. Three versions (2, 3, and 4) were built with distinctly different iron core radii as described in the callout. The internal diameter and copper coil remained constant throughout all versions of the final iteration.**

The final design used iron paint (49.97% wt) and solid iron wire (gauge 0.35 mm) to create an iron core external to a 5F catheter. The solenoid was wrapped around the dry core using 0.33 mm copper wire. In total, 9 prototypes were built, three at each discrete level of iron core weight. This allowed for analysis of the effect of iron core size on the strength of the magnetic field. This also allowed researchers to analyze the reliability of the manufacturing methods. Some variability was predicted between prototypes of the same level, but all three should behave more similarly to each other than the other groups.

# Chapter 3: Early Prototypes and Analysis of a Novel Fistula Occlusion Device

## *Methods*

The goal of this specific portion of the fistula occlusion device was to analyze a prototype that could move magnetically responsive material. Steel balls were used here for simplicity, in future studies, they will be replaced with ferromagnetic glue. The steel balls were an approximation of the ferromagnetic glue blob if it acted as a solid.

Prototypes were built according to the methods described in detail in chapter two. A Student's T-test assuming equal variances was performed on the iron core weights for each group of prototypes to determine sameness within a group and difference between groups. The solenoid coils were connected to a power supply in order to create the magnetic field.

### Horizontal Experiments

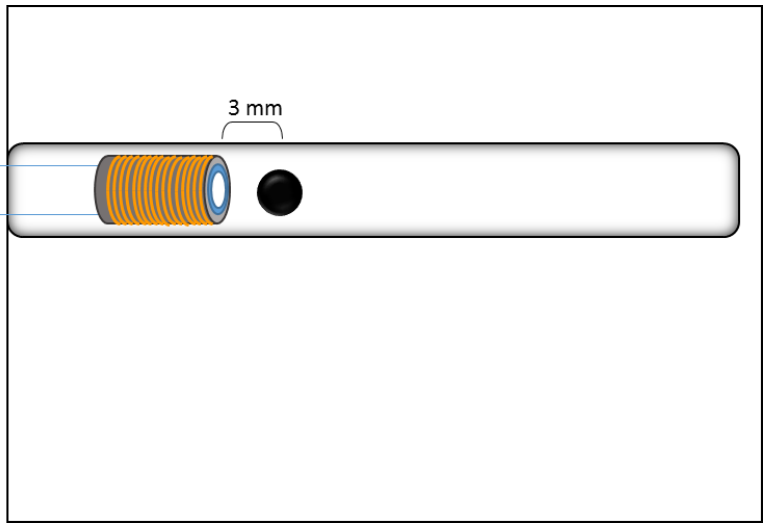


**Figure 8: Horizontal setup for evaluating the magnetic field of prototypes.**

Three sets of experiments were conducted to verify the presence of a magnetic field. In the first setup, each prototype was set in a slim track and secured as shown in Figure 8. A 3 mm steel ball was placed 3 mm away from the distal end of the solenoid and the power supply was turned on. The current through the external coil was increased until the magnetic field pulled the steel ball towards the solenoid. The voltage, current and power were recorded at

this instant. The power was turned off and the ball was returned to the start position. Every third trial the entire setup was redone to address potential setup bias. Nine trials were performed for each of the six prototypes in experimental groups 2 and 3. Group 4 was excluded from this experiment because its large size did not fit in the track. It also was much larger than the diameter of the steel ball used, so there was a greater discrepancy in the alignment which caused unreliable results.

## Vertical Experiments

In order to rectify problems with the first set up due to friction and alignment of the magnetic field, a second experimental set up was designed. Each prototype was secured vertically and connected to the power supply as shown in Figure 9. The power was turned to a maximum level of approximately 3A, and the 3 mm steel ball was allowed to hang off the distal end of the prototype. The power was turned down incrementally until the ball fell off. This experiment was used to determine feasibility of using a clinically applicable total weight. The third setup used two 3 mm steel balls weighing a combined total of 0.7427 g. It was determined through discussion with physicians who would potentially use this device that it needed to be able to lift 0.52 g. The experimental set up accounted for a 50% increase in glue weight. The same procedure was followed as in the second set of vertical experiments. 20 trials were attempted for each prototype.

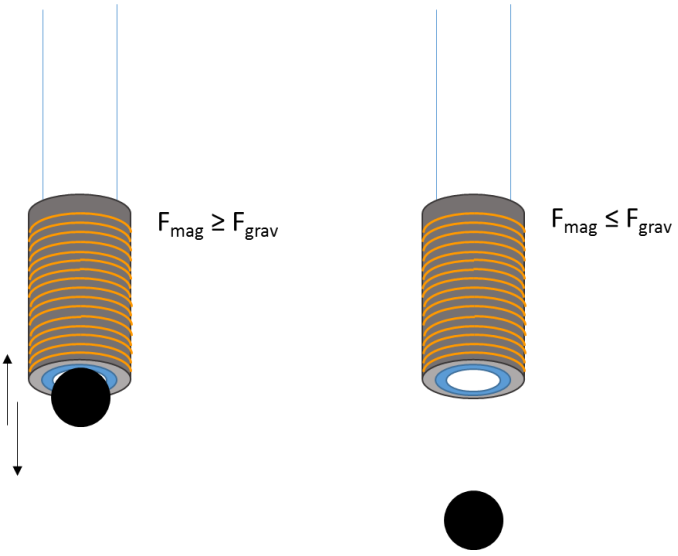


**Figure 9: Vertical experiment set up for evaluating prototypes.**

## *Results*

A Student's T-test assuming equal variances was performed on the iron core weights for each group of prototypes. Using $\alpha$=0.05, all groups were considered different from each other. Table 3 shows the results of these t-tests.

**Table 3: Results of the Student's T-test for equal variances between experimental groups 2 and 3, 3 and 4, and 2 and 4.**

| | **T-stat** | **T-crit** | **Result** |
|---|---|---|---|
| **2:3** | -18.126 | 2.776 | Reject |
| **3:4** | -20.055 | 2.776 | Reject |
| **2:4** | -34.63 | 2.776 | Reject |

## Horizontal Experiments

Nine prototypes (three of each construction) were built using the aforementioned method. 2 (A, B, C) had the smallest iron core, 3 (A, B, C) the middle and 4 (A, B, C) the largest. Each prototype moved the ball within the limits of the power supply, no more than 3A of current. Preliminary results indicate that solenoids on this scale can be used to move magnetically reactive materials. Initial results indicate that this design may provide a viable control mechanism for the deployment of magnetic glue. Figure 10-12 show the spread as well as the mean and standard deviation for each of the prototypes properly evaluated in the horizontal experimental setup.

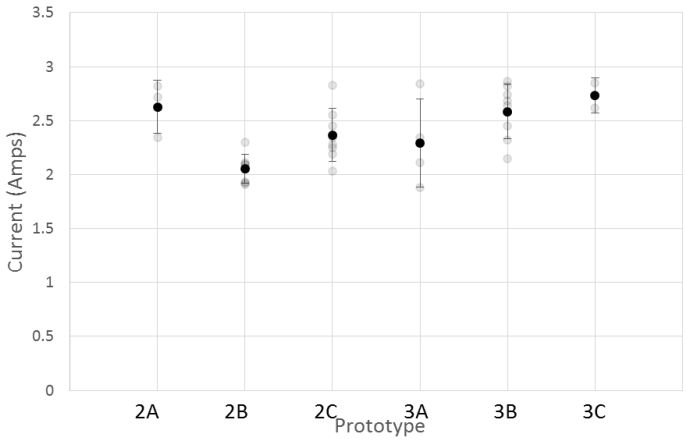


| Prototype # | Mean (A) | Standard Deviation |
|---|---|---|
| 2A | 2.62 | 0.25 |
| 2B | 2.05 | 0.13 |
| 2C | 2.37 | 0.25 |
| 3A | 2.29 | 0.41 |
| 3B | 2.58 | 0.25 |
| 3C | 2.73 | 0.16 |

**Figure 10: The current at which the ball moved for each trial in the horizontal experimental setup. The gray indicates the spread of values which explains the large standard deviations. The black is the mean and standard deviation for each prototype which can also be found in the table on the right.**

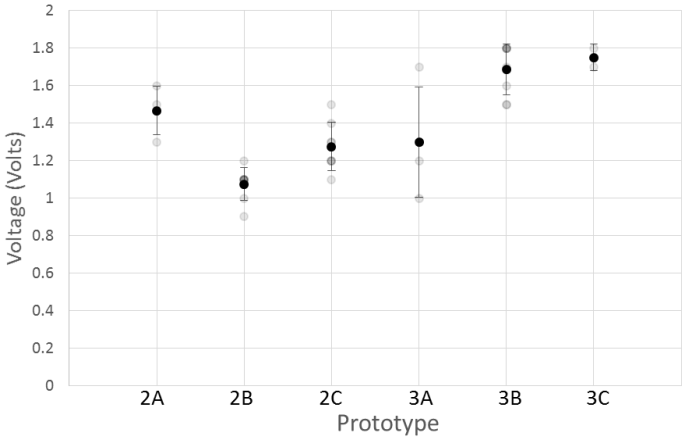


| Prototype # | Mean (V) | Standard Deviation |
|---|---|---|
| 2A | 1.46 | 0.15 |
| 2B | 1.08 | 0.09 |
| 2C | 1.28 | 0.13 |
| 3A | 1.30 | 0.29 |
| 3B | 1.69 | 0.14 |
| 3C | 1.75 | 0.07 |

**Figure 11: The voltage at which the ball moved for each trial in the horizontal experimental setup. The gray indicates the spread of values which explains the large standard deviations. The black is the mean and standard deviation for each prototype which can also be found in the table on the right.**

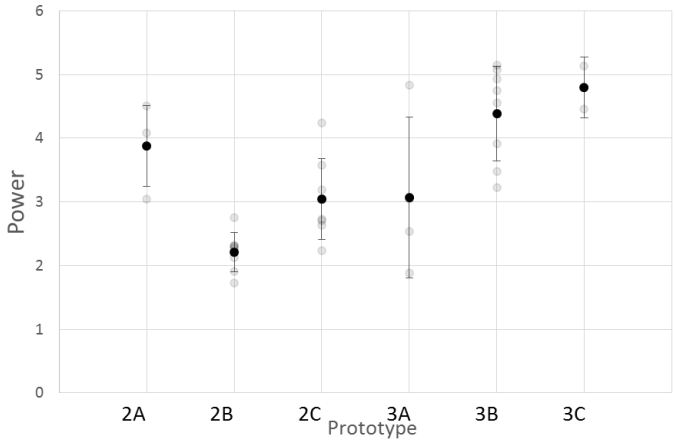


| Prototype # | Mean (W) | Standard Deviation |
|---|---|---|
| 2A | 3.89 | 0.76 |
| 2B | 2.21 | 0.31 |
| 2C | 3.04 | 0.63 |
| 3A | 3.07 | 1.26 |
| 3B | 4.39 | 0.75 |
| 3C | 4.79 | 0.48 |

**Figure 12: The power at which the ball moved for each trial in the horizontal experimental setup. The gray indicates the spread of values which explains the large standard deviations. The black is the mean and standard deviation for each prototype which can also be found in the table on the right.**

## Vertical Experiments

The next set of experiments used the same prototypes in a vertical position so that the magnetic force could be determined through a force balance as shown in equation 3.1.

(3.1) $$\sum F = ma = F_{magnet} - F_{gravity}$$

Prototypes 2A, 2B, 2C and 3B all failed to hold the 2 balls vertically and were thus excluded from the results. Figures 13-15 show similar spread and mean with standard deviation as in Figures 10-12.

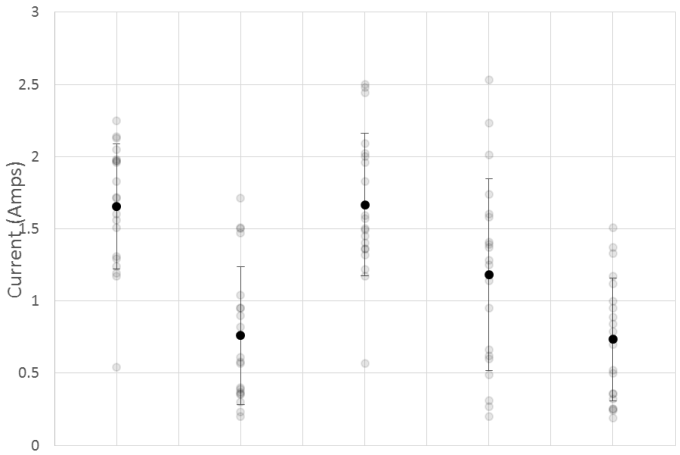


| Prototype # | Mean (A) | Standard Deviation |
|---|---|---|
| 3A | 1.66 | 0.43 |
| 3B | n/a | n/a |
| 3C | 0.76 | 0.48 |
| 4A | 0.73 | 0.42 |
| 4B | 1.18 | 0.67 |
| 4C | 1.66 | 0.49 |

**Figure 13: The current at which the 2 balls were no longer held on by sufficient magnetic force provided by the solenoid. The gray indicates the spread of values which explains the large standard deviations. The black is the mean and standard deviation for each prototype which can also be found in the table on the right.**

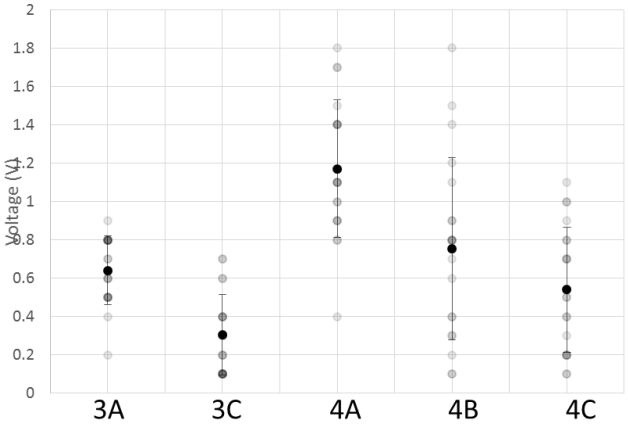


| Prototype # | Mean (V) | Standard Deviation |
|---|---|---|
| 3A | 0.31 | 0.21 |
| 3B | n/a | n/a |
| 3C | 0.64 | 0.18 |
| 4A | 0.54 | 0.33 |
| 4B | 0.76 | 0.48 |
| 4C | 1.17 | 0.36 |

**Figure 14: The voltage at which the 2 balls were no longer held on by sufficient magnetic force provided by the solenoid. The gray indicates the spread of values which explains the large standard deviations. The black is the mean and standard deviation for each prototype which can also be found in the table on the right.**

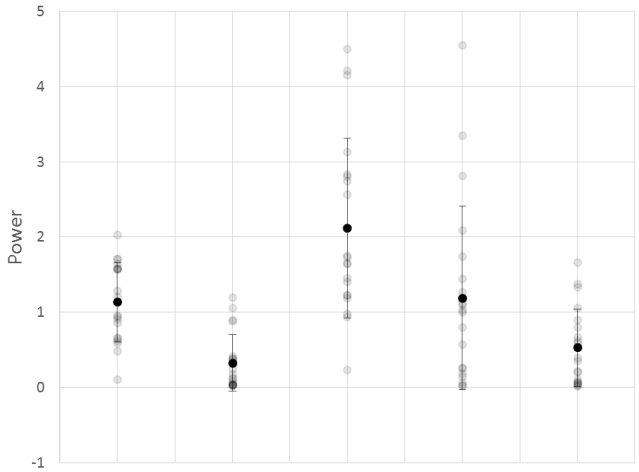


| Prototype # | Mean (A) | Standard Deviation |
|---|---|---|
| 3A | 1.13 | 0.52 |
| 3B | n/a | n/a |
| 3C | 0.33 | 0.38 |
| 4A | 0.53 | 0.51 |
| 4B | 1.20 | 1.22 |
| 4C | 2.12 | 1.20 |

**Figure 15: The power at which the 2 balls were no longer held on by sufficient magnetic force provided by the solenoid. The gray indicates the spread of values which explains the large standard deviations. The black is the mean and standard deviation for each prototype which can also be found in the table on the right.**

## *Discussion*

This work represents the beginning of a body of work to develop a device to repair fistulas. This study was limited by the resolution of the available power supply and the ability to control the alignment of each prototype into the track. Researchers could also not control for friction within the track, although all attempts were made to reduce friction as much as possible. Vertical experiments allowed the research team to focus solely on overcoming the gravitational force. However, further iterations of the prototypes need to be developed in order to validate the trends seen here as well as hopefully provide a more predictable force on the ball.

In all of the trials and conditions, the variability was interesting to note. Although some variability is expected, drastic outliers are not. The outliers could be the effect of changes in the system that were uncontrolled or unidentifiable by the research team. Additionally, although trend lines could not be established due to the high variability, it was expected that there would be a relationship between the iron core weight and the required current to move the ball. However, the

results were inconsistent between trials and prototype groups indicating an issue with either alignment, resolution of the power supply or variability in the device construction. Reliability needs to be addressed in the experimental set up before making general conclusions. However, it does demonstrate that magnetic force can be achieved at this scale.

Additionally, the magnetic glue will need to be characterized. This is important so that the flow patterns are understood when being deployed. Although previous research indicates the applicability of fibrin glue to this scenario, it is unknown if the addition of ferrous particles will alter its composition. Evaluating different glue ratios in combination with solenoid catheters will help to fine-tune the design parameters of both components. The fluid mechanics of the system are the next major obstacle for designing a prototype to work in unison. The experiments will have to be repeated in order to fully understand the ramifications of the fluid mechanics in a magnetic field.

The method of creating a solenoid-catheter described here provides a promising foundation for future iterations of the device. Further verification is needed before conclusions can be drawn regarding the usefulness of the design.

# Chapter 4: Computational Model of a Novel Fistula Occlusion Device

## *Methods*

In order to optimize the physical prototype of the fistula occlusion device, a computational model was developed. This model allows for greater manipulation of design parameters than iterating individual prototypes. The goal was to validate the model using experimental results seen in chapter 3. The model was constructed using MATLAB R2014a assuming two concentric semi-infinite cylinders. Cylinder A represents the iron core, and cylinder B is the hollow lumen as shown in Figure 16.

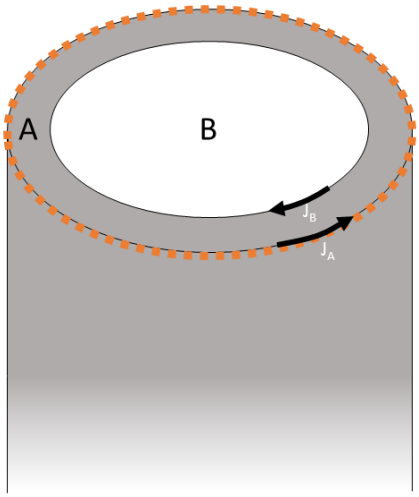


**Figure 16: Surface currents for two cylinders created in computational model. $J_A$ corresponds to the current induced on the external surface of the iron core, and $J_B$ is the inside surface of the iron core. The orange dotted line is representative of the solenoid coil.**

The copper solenoid is built around the outermost cylinder. Equation 4.1 is the equation for describing magnetic flux density, B [52].

(4.1)
$$\boldsymbol{B}\ \bar{r}\ = \frac{\mu_0}{4\pi}\iint_S \frac{\boldsymbol{J}_s\ \vec{r}\ \times\ \bar{r} - \vec{r}}{\left|\bar{r} - \vec{r}\right|^3} ds'$$

Where $\mathbf{J_s}$ is a summation of the alternating surface currents, $J_A$, and $J_B$ on the external side of each corresponding cylinder. Surface currents are a fictional representation of the magnetic effects produced by the solenoid on the magnetic material and used to calculate the overall magnetic field strength. Substitutions were applied in order to perform a Taylor series expansion around a, the point at which the field was evaluated. This expansion assumes that *a* is much smaller than *x*, *y*, and *z*. This assumption was made in order to avoid a numerical methods approximation. After integrating over the surface the resultant vectors were put back into equation 4.1. Although magnetic flux density, **B**, is indicative of the force it does not explain all of the phenomena.

To solve for the magnetic field, H, equation 4.2 was used, where $\mu_0$ is the permeability of free space.

(4.2) $$\mathbf{H}(\vec{\mathbf{r}}) = \frac{\mathbf{B}(\vec{\mathbf{r}})}{\mu_0}$$

$\mathbf{H}(\vec{\mathbf{r}})$ and its derivative $\nabla\mathbf{H}(\vec{\mathbf{r}})$ , can be used to describe the force felt by a particle of volume, *v*, *a* distance away from the magnetic source. Equation 4.3 explicitly describes the closed-form solution for F.

(4.3) $$\vec{\mathbf{F}} = \mu_0(\mu_p - 1) \times \vec{\mathbf{H}}(\vec{r}) \bullet \nabla\vec{\mathbf{H}}(\vec{r}) \times \Delta v$$

$\mu_p$ is the relative permeability for the particle being acted upon. Once calculated, the force can be compared to the force of gravity.

All calculations were performed on an x-z grid from -10 radius to +10 radius skipping a square of -1 radius to +1 radius. As the particle moves closer and closer to the tip of the solenoid (the origin) the magnetic forces approach infinity and cause singular solutions. Therefore, it was necessary to remove this area from the calculation.

## *Results*

### Validation and Verification

The initial results show the progression of the model through the calculations. The parameters were defined as shown in table 4. These, along with equations 4.1-4.3 allowed for development of the model.

**Table 4: Inputs for computational model. During parametric analysis variables with a * changed.**

| **Parameter** | **Value** | **Units** |
|---|---|---|
| Current, i* | 2 | A |
| Permeability of free space, $\mu_0$ | $4\pi^{-7}$ | |
| Permeability of solenoid* | 5000 | |
| Permeability of glue | 50 | |
| Number of turns | 250 | 1/m |
| Outer radius, c* | 3.86 | mm |
| Inner radius, p | 0.98 | mm |
| Volume of particle, v | 1 | mL |

The model was verified by ensuring that if c=p, or there was no iron core present, that the magnetic field went to 0. This is because the surface currents from each set of terms would cancel. Additionally, when the double integral portion of equation 4.1 is evaluated 1 radii away from the origin, i.e. : it becomes close to 1, the magnetic flux density, B, should be equal to $J_s/4\pi$. This was seen in the calculations and therefore it was determined that the model was producing results consistent with the mathematical formulations.

Figure 17 shows the magnetic flux density of the computational model with an overlay of a solenoid. This shape is consistent with solenoid field theory [41,45,53]. Since the model is semi-infinite, the magnetic field is greatest along the edges of the solenoid and dramatically decreases as a function of r in both the x and z directions.

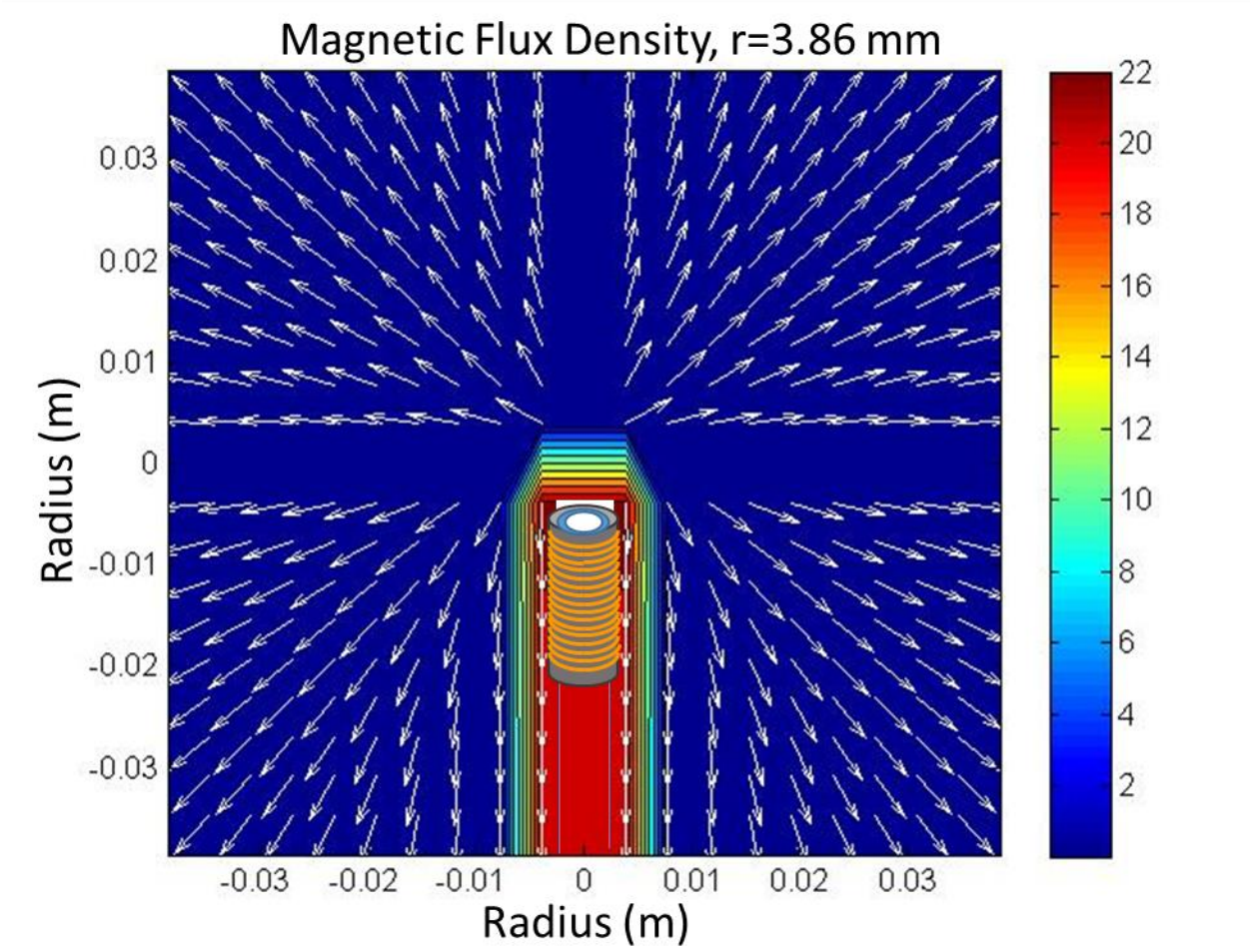


**Figure 17: Magnetic flux density of a solenoid with radius 3.86 mm, assuming an input current of 2 A and a solenoid core permeability of 500. A schematic of the prototype is overlaid to show where the solenoid is in relation to the field.**

Figure 18 is Figure 17 plotted on a decibel scale. This shows the change in orders of magnitude as you move farther and farther away from the origin.

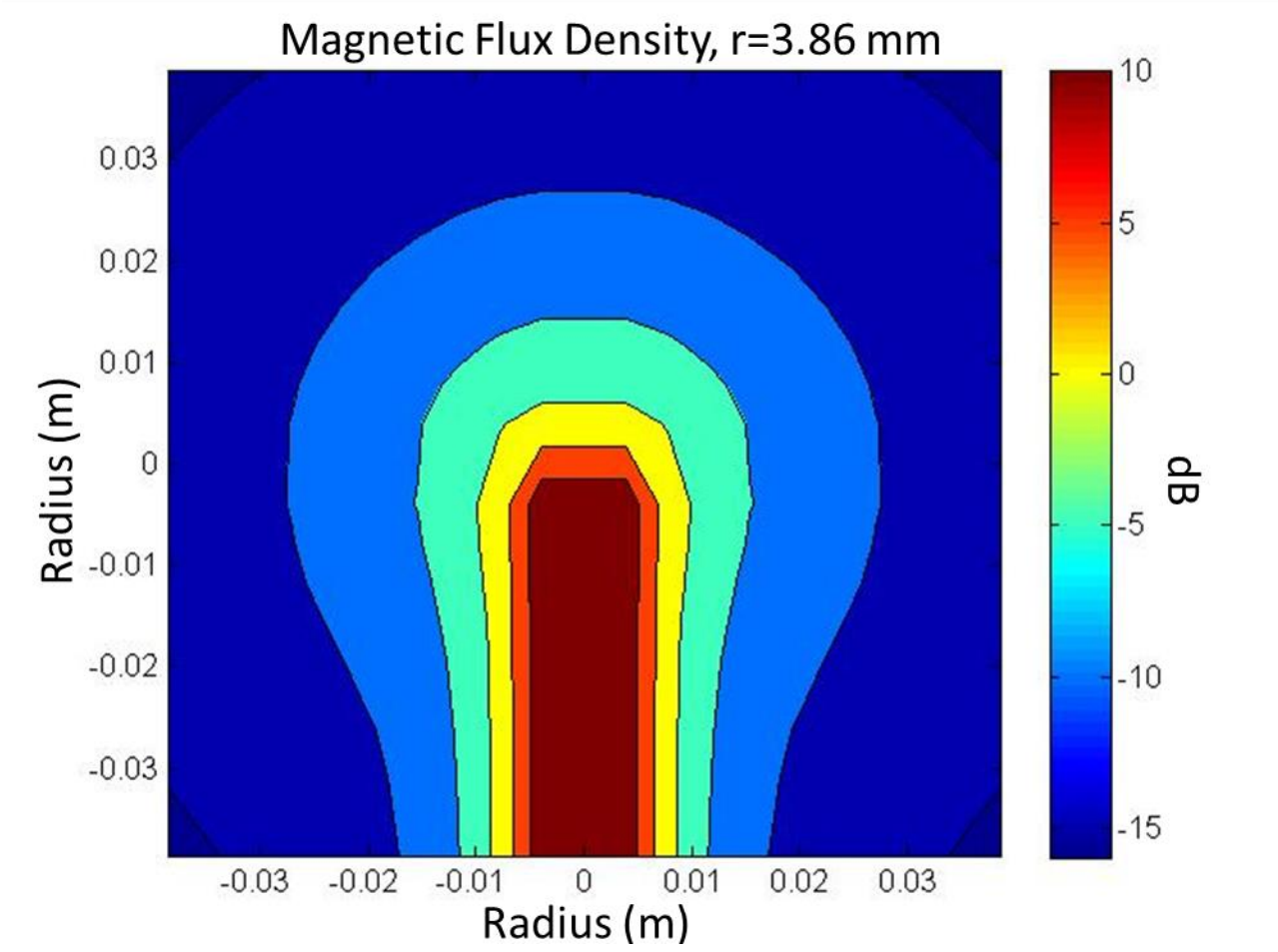


**Figure 18: Magnetic flux density of the same prototype shown on a decibel scale.**

The magnetic field was found to be between the order of refrigerator magnets (5 mT) and neodymium rare earth magnets (1.25 T) and therefore considered sufficient for this application [54,55]. These values fall between the yellow and light blue regions shown on Figure 18.

The magnetic flux density was divided by the permeability of free space (Equation 4.2) in order to determine the magnetic field strength as shown in Figure 19.

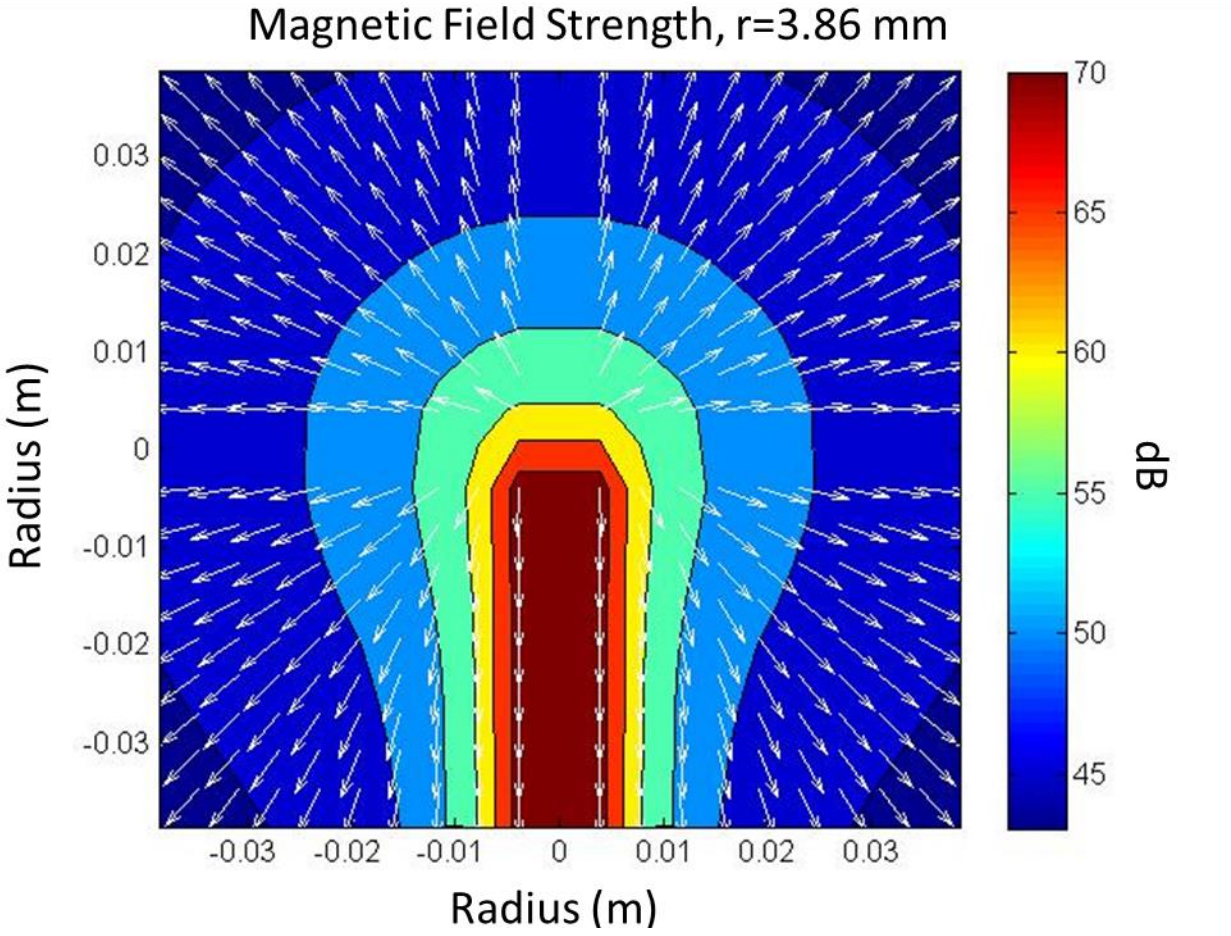


**Figure 19: Magnetic field strength of prototype with radius 3.86 mm, assuming an input current of 2 A and a solenoid core permeability of 500 on a decibel scale.**

## Parametric Analysis

The goal of this model was to develop a computational method for optimizing design parameters. The variables that could change were: c, i, and μ. Two parametric analyses were performed in order to identify the best assembly of parameters. The parametric plots are shown in full in Appendix C.

The first parametric analysis held the current, i, constant at 2 A. The outer radius, c, and permeability, μ, were varied independently. Physically, μ, is a constant defined by the material properties of the core. However, since the core in the prototypes described in chapter 2 is composed

of an imperfect iron paint and iron wire combination, an exact permeability could not be determined. It is believed that it falls somewhere between 50 and 5,000. Trials were completed at μ equals 50, 500 and 5,000 for this analysis. 5,000 is the permeability of pure iron and the ideal scenario. Additionally, a trial was performed for each discrete radii, 1.17 mm, 2.35 mm and 3.86 mm at each level of permeability for 9 total scenarios.

The second parametric analysis assumed a constant permeability of 500 and varied the current, i, at 0.02 A, 0.2 A, and 2 A, and the outer radius, c, as in the first analysis. This resulted in 6 additional scenarios and 3 that were repeated from the first parametric analysis.

## *Discussion*

The profiles of the magnetic flux density and magnetic field strength are consistent with solenoid theory. As you move away from the tip of the solenoid the magnetic field breaks down rapidly. Additionally, all forces point towards the tip where the magnetic field is the strongest. Far away from the solenoid the field is zero.

The parametric analysis of the model shows that as the permeability or current increases the magnetic field increases in strength. It also increases as the thickness of the iron core increases, however, by a lesser amount.

It should be noted that this approximation is more valid the smaller the volume of the particle is. As $\Delta v$ increases, the model breaks down because the magnetic field cannot be approximated as constant. Although different values of $\Delta v$ were examined, the results presented here are for 1 mL particles due to this approximation.

The results of this model show that it is feasible to predict the magnetic field produced by a solenoidal source. However, more realistic conditions need to be taken into account in order for the model to closely match what is seen experimentally. Additionally, future work is needed in

order to translate the magnetic field strength to a tangible magnetic force calculation. At that point it will become much more valuable to the development of the device.

# Chapter 5: Conclusions and Future Work

The research conducted in the previous chapters is a first step towards creating a fistula occlusion device that could benefit patients worldwide. The conclusions drawn from both the physical experiments and the computational model are beneficial in advising design decisions going forward. Additionally, the design process has allowed for creative iterations. However, the current work is not without limitations. Some of these limitations are anticipated to be addressed in future work. Other future steps include completing the necessary safety and efficacy experiments for FDA approval processes.

A major accomplishment for this thesis was demonstrating that it is feasible to produce magnetic fields at this scale that deliver sufficient force for the task. This was shown through the vertical experiments that are 50% more weight than what should be required clinically. Although precision is a concern, the binary success rate was greater than the failure rate and can be refined in the future.

Also, a hollow core solenoid is novel. Most literature cites solenoids that have solid iron cores [43,45]. The clinical application shown here requires a hollow solenoid. The glue needs to be able delivered to the fistula site using a catheter and the catheter must be positioned using a guidewire. Those design requirements dictate the geometric shape of the core. Showing that magnetic forces can be achieved at both a small scale and from a hollow core are foundational to the further development of this device.

From the model, the biggest accomplishment was establishing a working model to test design parameters before building them. This will allow the team to better predict the effect of different design parameters on the overall magnetic field. Additionally, the model provides a visual

for geometric data. It allows the team to identify how close the glue plug needs to be to the tip of the catheter to still be affected by the magnetic field.

These conclusions are significant as this thesis is the beginning of an ongoing research project. A preliminary patent has already been filed for both the electromagnetic catheter and the glue composition (July 2015).

## *Current Limitations*

There are two major limitations to the current design. First off, fluid mechanics of the glue have not been addressed at all. The fluid mechanics of the cyanoacrylate-ferrofluid solution are complex and may change the effectiveness of the prototype significantly. All of the work presented here has assumed solid steel spheres that do not change shape. Cyanoacrylate will change shape as a function of time and in the presence of a magnetic field. Additionally, the material properties of the ferrofluid-cyanoacrylate mixture will not remain constant which could affect the validity of the conclusions made on solid spheres. Solid spheres were used for this preliminary work because of their ease of use. It allowed the researcher to focus on developing only one component of the fistula repair system, the electromagnetic catheter, instead of controlling all components at once.

Second, all of the prototypes were handmade. Although great care was taken when building each iron core and solenoid, variability exists in the prototypes due to the manufacturing process. Although measurements were taken in regards to the weight of each core and they are statistically the same, slight differences in geometry or particle distribution could have occurred. Since the copper wire was wound securely around each core after drying, any differences in geometry would be confounded with the application of the solenoid and could be the cause of the alignment problems seen in the horizontal experiments of chapter 2. Ignoring fluid mechanics and the

manufacturing processes are both limits to the success of the research, however, that does not negate the significance of the results presented previously.

Additionally, the computational model has some limitations in its accuracy. The magnetic force and magnetic field could not be calculated at points near the tip. In electromagnetics, as you approach the source the fields become singular which complicates the mathematics and makes them nearly impossible to solve. For this model we avoided this by only considering fields a sufficient ways away, i.e.: greater than 1 radius. This is not the best approximation since the application for which the device is being used for relies on the near field.

The Taylor series expansion that was used to solve for the magnetic flux density relies on the assumption that the particle is far away from the source. As it gets closer the assumption tends to break down. The model truncates the expansion at the 3$^{rd}$ order. Terms of higher order made negligible impact on the results and were therefore not included. The alternative to a Taylor series approximation is to go to numerical methods, however that would not lead to a closed form solution. Both the experiments and model have limitations in their conclusiveness which will be addressed in future work.

## *Future Work*

The limitations presented are influential towards formulating the next steps in this research project. The work present in this thesis are the foundation for creating a novel fistula occlusion device that could be used worldwide to increase quality of life for patients. There are three next steps that answer to the limitations described earlier and three other steps that move the project towards the ultimate goal: in-patient use.

The exact composition of the glue needs to be explored. Although previous research indicates ferrofluids will stay in solution when combined with other liquids, this exact scenario

has not yet been analyzed [38]. Determining the properties of this novel glue will go a long way towards increasing the accuracy in the computational model and the experimental set up. It is known that dramatic viscosity changes occur in both cyanoacrylate as it cures and in ferrofluid in the presence of a magnetic field [31,32]. Up to this point the differences between solid and fluid mechanics have been ignored. This is simply not accurate and a significant assumption in the research. It simplified the manufacturing of the initial prototypes as well as allowed the team to focus on one part of the delivery system as opposed to two. Now, they must be combined in order to determine full feasibility of the product.

The catheter portion of the system needs professional manufacturing. It is believed that precise manufacturing of the iron core and copper solenoid coil will increase the reliability and accuracy of the prototypes. There is significant room for improvement and refinement in the build of each device although great care was taken in details of the prototypes. For example, the iron core could be built out of solid iron rather than an iron paint and iron wire combination. In the next step of prototype development, the manufacturing will be outsourced so that increased analysis can be performed.

One of the major limitations of the computational model was that it ignored the fields induced in the particles. The future of the model will be to include a 3$^{rd}$ cylinder, replacing the lumen, with the magnetic glue. This will create a 3$^{rd}$ surface current and ultimately change the magnetic field shape and intensity. Hopefully this change will also allow the team to understand how far the glue can be pushed out of the catheter while still retaining its cylindrical shape.

After the glue and manufacturing concerns have been addressed, there are still several studies necessary in order to be prepared for clinical trials. The most obvious is to repeat the experiments described in Chapter 3 with the newly developed glue instead of the steel balls. The

results of which will validate the previous experiments. Additionally this will allow the research team to make final design decisions regarding the deployment system. These experiments will provide information regarding the finalization of the design parameters, current, number of turns, and core composition.

In regards to the core, beyond size, the material can be changed. Iron is the most common material used in solenoids because of its availability and excellent permeability. However, other materials exist that may provide better results for the forces we are requiring in such a small space. Further investigation is needed to know if iron is the proper choice for the core in this application or if changing the material would create the magnetic fields desired.

Lastly, after the technical problems have been addressed and further clarified, cadaveric and animal studies need to be conducted. Although there is not a preferred animal model for these types of studies, dogs have been used previously for gastrointestinal defect surgeries [56]. Dogs likely represent the best model for assessing this product. After the final prototype has been built, it will be assessed for performance in an animal model. Physicians will use the device as intended for human patients. Additionally, mechanical testing will be performed on the repaired tissue to ensure the adhesive qualities of the glue are up to par. With positive results in a series of animal tests and no unforeseen side effects, the device could potentially be used in patients.

## *Conclusion*

The preliminary findings described here are promising in the feasibility of developing a novel fistula occlusion device. Although complete validation and verification of the prototype forces is incomplete at this time, major progress has been made towards creating a viable prototype. Additional iterations of the computational model will allow the team to determine the ideal design parameter values for the final prototypes. These devices will be manufactured

professionally for extensive mechanical and behavioral testing. Afterwards, pending successful analysis, they will be used in cadaveric and animal trials as described in *future work*.

# References


[1] Vallejo, E. C., Martinez-Galdamez, M., Del Olmo Martínez, L., Brunet, E. C., and Martin, E. S., 2015, "Percutaneous treatment of a duodenocutaneous high-flow fistula using a new biological plug," Diagn. Interv. Radiol., **21**(3), pp. 247–251.

[2] Šebek, M., MUDr Tomáš, 2008, Čeština: Crohnova nemoc - postižení více vrstev střevní sliznice, tvorba píštělí.

[3] "Gastrointestinal fistula: MedlinePlus Medical Encyclopedia" [Online]. Available: https://www.nlm.nih.gov/medlineplus/ency/article/001129.htm. [Accessed: 28-Mar-2016].

[4] Ozer, M. T., Coskun, A. K., Ozerhan, I. H., Ersoz, N., Yildiz, R., Sinan, H., Demirbas, S., Kozak, O., Uzar, A. I., and Cetiner, S., 2011, "Use of vacuum-assisted closure (VAC$^{TM}$) in high-energy complicated perineal injuries: analysis of nine cases," Int. Wound J., **8**(6), pp. 599–607.

[5] Teitelbaum, J. E., Gorcey, S. A., and Fox, V. L., 2005, "Combined endoscopic cautery and clip closure of chronic gastrocutaneous fistulas," Gastrointest. Endosc., **62**(3), pp. 432–435.

[6] Lyon, J. W., Hodde, J. P., Hucks, D., and Changkuon, D. I., 2013, "First Experience with the Use of a Collagen Fistula Plug to Treat Enterocutaneous Fistulas," J. Vasc. Interv. Radiol., **24**(10), pp. 1559–1565.

[7] Eskaros, S., Ghevariya, V., Krishnaiah, M., Asarian, A., and Anand, S., 2009, "Percutaneous endoscopic suturing: an effective treatment for gastrocutaneous fistula," Gastrointest. Endosc., **70**(4), pp. 768–771.

[8] Joyce, M. R., and Dietz, D. W., 2009, "Management of complex gastrointestinal fistula," Curr. Probl. Surg., **46**(5), pp. 384–430.

[9] Parks, A. G., Gordon, P. H., and Hardcastle, J. D., 1976, "A classification of fistula-in-ano," Br. J. Surg., **63**(1), pp. 1–12.

[10] Law, R., Song, L. M. W. K., Irani, S., and Baron, T. H., 2014, "Immediate technical and delayed clinical outcome of fistula closure using an over-the-scope clip device," Surg. Endosc., **29**(7), pp. 1781–1786.

[11] Teixeira, P. G. R., Inaba, K., Dubose, J., Salim, A., Brown, C., Rhee, P., Browder, T., and Demetriades, D., 2009, "Enterocutaneous Fistula Complicating Trauma Laparotomy: A Major Resource Burden," Am. Surg., **75**(1), pp. 30–32.

[12] Owen, G., Keshava, A., Stewart, P., Patterson, J., Chapuis, P., Bokey, E., and Rickard, M., 2010, "Plugs unplugged. Anal fistula plug: the Concord experience," ANZ J. Surg., **80**(5), pp. 341–343.

[13] "Bioprosthetic Plugs for Complex Anal Fistulas: An Early Experience" [Online]. Available: http://www.sciencedirect.com/science/article/pii/S0149794406001309. [Accessed: 04-Apr-2016].

[14] Papavramidis, S. T., Eleftheriadis, E. E., Papavramidis, T. S., Kotzampassi, K. E., and Gamvros, O. G., 2004, "Endoscopic management of gastrocutaneous fistula after bariatric surgery by using a fibrin sealant," Gastrointest. Endosc., **59**(2), pp. 296–300.

[15] "Surgical management of high output enterocutaneous fistulae:... : Current Opinion in Clinical Nutrition & Metabolic Care," LWW [Online]. Available: http://journals.lww.com/co-clinicalnutrition/Fulltext/2004/05000/Surgical_management_of_high_output_enterocutaneous.11.aspx. [Accessed: 04-Apr-2016].

[16] Amrani, S., Zimmern, A., O'Hara, K., and Corman, M. L., 2008, "The Surgisis® AFP™ anal fistula plug: a new and reasonable alternative for the treatment of anal fistula," Gastroentérologie Clin. Biol., **32**(11), pp. 946–948.
[17] Stamos, M. J., Snyder, M., Robb, B. W., Ky, A., Singer, M., Stewart, D. B., Sonoda, T., and Abcarian, H., 2015, "Prospective Multicenter Study of a Synthetic Bioabsorbable Anal Fistula Plug to Treat Cryptoglandular Transsphincteric Anal Fistulas:," Dis. Colon Rectum, **58**(3), pp. 344–351.
[18] Draus Jr, J. M., Huss, S. A., Harty, N. J., Cheadle, W. G., and Larson, G. M., 2006, "Enterocutaneous fistula: Are treatments improving?," Surgery, **140**(4), pp. 570–578.
[19] Büyükyavuz, I., Karnak, I., Yiğit, S., and Tanyel, F. C., 2004, "Successful treatment of enterocutaneous fistula in a premature newborn by using octreotide," Turk. J. Pediatr., **46**(3), pp. 289–291.
[20] Tachi, M., and Hirabayashi, S., 2002, "Enterocutaneous Fistula Treated With a Fasciocutaneous Turnover Flap:," Ann. Plast. Surg., **48**(5), pp. 554–556.
[21] Kumta, N. A., Boumitri, C., and Kahaleh, M., 2015, "New devices and techniques for handling adverse events: claw, suture, or cover?," Gastrointest. Endosc. Clin. N. Am., **25**(1), pp. 159–168.
[22] Adamina, M., Hoch, J. S., and Burnstein, M. J., 2010, "To plug or not to plug: A cost-effectiveness analysis for complex anal fistula," Surgery, **147**(1), pp. 72–78.
[23] Leng, Q., and Jin, H.-Y., 2012, "Anal fistula plug vs mucosa advancement flap in complex fistula-in-ano: A meta-analysis," World J. Gastrointest. Surg., **4**(11), pp. 256–261.
[24] Shand, A., Reading, S., Ewing, J., Neil, B., Welsh, D., Parker, A., and Ghosh, S., 1997, "Palliation of a malignant gastrocolic fistula by endoscopic human fibrin sealant injection," Eur. J. Gastroenterol. Hepatol., **9**(10), pp. 1009–1011.
[25] Chung, W., Kazemi, P., Ko, D., Sun, C., Brown, C. J., Raval, M., and Phang, T., 2009, "Anal fistula plug and fibrin glue versus conventional treatment in repair of complex anal fistulas," Am. J. Surg., **197**(5), pp. 604–608.
[26] Eaglstein, W. H., and Sullivan, T., 2005, "Cyanoacrylates for Skin Closure," Dermatol. Clin., **23**(2), pp. 193–198.
[27] Love, L. J., Jansen, J. F., McKnight, T. E., Roh, Y., Phelps, T. J., Yeary, L. W., and Cunningham, G. T., 2005, "Ferrofluid field induced flow for microfluidic applications," IEEEASME Trans. Mechatron., **10**(1), pp. 68–76.
[28] Melikhov, Y., Lee, S. J., Jiles, D. C., Schmidt, D. H., Porter, M. D., and Shinar, R., 2003, "Microelectromagnetic ferrofluid-based actuator," J. Appl. Phys., **93**(10), pp. 8438–8440.
[29] Rahmani, A. R., Prodanović, M., Bryant, S. L., and Huh, C., 2012, "Quasi-static analysis of a ferrofluid blob in a capillary tube," J. Appl. Phys., **111**(7), p. 074901.
[30] Sánchez, J. H., and Rinaldi, C., 2010, "Magnetoviscosity of dilute magnetic fluids in oscillating and rotating magnetic fields," Phys. Fluids 1994-Present, **22**(4), p. 043304.
[31] Borin, D., and Odenbach, S., 2011, "Rheology of novel ferrofluids," Int. J. Mod. Phys. B, **25**(07), pp. 963–969.
[32] Nowak, J., Wolf, D., and Odenbach, S., 2014, "A rheological and microscopical characterization of biocompatible ferrofluids," J. Magn. Magn. Mater., **354**, pp. 98–104.
[33] Müller, O., Hahn, D., and Liu, M., 2006, "Non-Newtonian behaviour in ferrofluids and magnetization relaxation," J. Phys. Condens. Matter, **18**(38), p. S2623.

[34] Mériguet, G., Dubois, E., Jardat, M., Bourdon, A., Demouchy, G., Dupuis, V., Farago, B., Perzynski, R., and Turq, P., 2006, "Understanding the structure and the dynamics of magnetic fluids: coupling of experiment and simulation," J. Phys. Condens. Matter, **18**(38), p. S2685.
[35] Shahnazian, H., and Odenbach, S., 2007, "Yield stress in ferrofluids?," Int. J. Mod. Phys. B, **21**(28n29), pp. 4806–4812.
[36] "Love_Ferrofluid field induced flow for microfluidic.pdf."
[37] Mefford, O. T., Woodward, R. C., Goff, J. D., Vadala, T. P., St. Pierre, T. G., Dailey, J. P., and Riffle, J. S., 2007, "Field-induced motion of ferrofluids through immiscible viscous media: Testbed for restorative treatment of retinal detachment," J. Magn. Magn. Mater., **311**(1), pp. 347–353.
[38] Thiele, R. H., Colquhoun, D. A., Gillies, G. T., and Tiouririne, M., 2012, "Manipulation of Hyperbaric Lidocaine Using a Weak Magnetic Field: A Pilot Study," Anesth. Analg., **114**(6), pp. 1365–1367.
[39] Paschalis, E. I., Chodosh, J., Sperling, R. A., Salvador-Culla, B., and Dohlman, C., 2013, "A Novel Implantable Glaucoma Valve Using Ferrofluid," PLOS ONE, **8**(6), p. e67404.
[40] Dugdale, D., 1993, Essentials of Electromagnetism, The Macmilln Press Ltd, Houndmills, Basingstoke, Hampshire, London.
[41] Garg, A., 2012, Classical Electromagnetism in a Nutshell, Princeton University Press.
[42] Burke, H. E., 1986, Handbook of Magnetic Phenomena, Von Nostrand Reinhold Company Inc, New York, New York.
[43] De Wolf, D. A., 2001, Essentials of Electromagnetics For Engineering, Cambridge University Press, Cambridge UK.
[44] Lorrain, P., and Corson, D. R., 1978, Electromagnetism: Principles and Applications, W. H. Freeman and Company, USA.
[45] Inan, U. S., and Inan, A. S., 1999, Engineering Electromagnetics, Addison Wesley Longman Inc, Menlo Park, CA.
[46] Wang, Z., Brown, A., Andr&#xe9, Pascal, Brown, S. I., Florence, G. J., and Cuschieri, A., 2013, "Magnetic Retraction of Bowel by Intraluminal Injectable Cyanoacrylate-Based Magnetic Glue," BioMed Res. Int., **2013**, p. e526512.
[47] "Magnetic force of a solenoid.pdf."
[48] He, W., Lee, S. J., Jiles, D. C., Schmidt, D. H., Porter, M. D., and Shinar, R., 2003, "Design of high-magnetic field gradient sources for controlling magnetically induced flow of ferrofluids in microfluidic systems," J. Appl. Phys., **93**(10), pp. 7459–7461.
[49] Freeman, J. R., 1979, Controlling Magnetic Field Profiles, Department of Energy, Sandia Laboratories.
[50] "TRUFILL n-Butyl Cyanoacrylate LIquid Embolic System."
[51] 2009, "Modern Masters Material Safety Data Sheet."
[52] Conway, J. T., 2001, "Exact solutions for the magnetic fields of axisymmetric solenoids and current distributions," IEEE Trans. Magn., **37**(4), pp. 2977–2988.
[53] Geek3, 2010, English: Diagram of a solenoid's magnetic field.
[54] "mritechnique" [Online]. Available: http://www.nevusnetwork.org/mritech.htm. [Accessed: 11-Apr-2016].
[55] Ivanova, G., 2007, "The Tesla: SI Unit of Magnetic Field," Tesla Radio Conspir.
[56] Cui, X., Lei, P., Liu, S., Liu, X., Wu, Z., and Lv, Y., 2015, "A sutureless method for digestive tract reconstruction during pancreaticoduodenectomy in a dog model," Int. J. Clin. Exp. Med., **8**(1), pp. 289–296.

## Appendix A---Math Model

This appendix covers the derivation of the computational model used in chapter 4. The goal was to develop an explicit form of the equations governing the magnetic field. N & I are inputs to the model describing the current and turns/meter of the solenoid external to the core. Js is the fictitious representation of a surface current created by I in the paramagnetic material. H(r) is the magnetic field pointing in the z direction measured in A/m. B(r) is the magnetic flux density produced by the solenoid. $B_0$ is for the flux density corresponding to the surface of the glue cylinder. $B_1$ corresponds to the internal surface of the core and $B_2$ is the external surface of the core. Later, these will be combined to describe the entire system.

$$N \doteq \text{Turns / meter}$$

$$I \doteq \text{Current in Amps}$$

$$J_s = N I$$

$$\mathbf{H}(\bar{r}) = J_s \hat{\mathbf{z}} \quad A/m$$

$$\mathbf{B}_0(\bar{r}) = \mu_0 J_s \hat{\mathbf{z}} \quad W/m^2$$

$$\mathbf{B}_1(\bar{r}) = \mu_1^r \mu_0 J_s \hat{\mathbf{z}} = \mu_1^r \mathbf{B}_1(\bar{r}) \hat{\mathbf{z}} \quad W/m^2$$

$$\mathbf{B}_2(\bar{r}) = \mu_2^r \mu_0 J_s \hat{\mathbf{z}} = \mu_2^r \mathbf{B}_2(\bar{r}) \hat{\mathbf{z}} \quad W/m^2$$

$$\mathbf{M}_1(\bar{r}) = \left(\mu_1^r - 1\right)\mathbf{H}(\bar{r}) = \left(\mu_1^r - 1\right)J_s\,\hat{\mathbf{z}} \cong \mu_1^r\,J_s\,\hat{\mathbf{z}} \quad A/m$$

$$\mathbf{M}_2(\bar{r}) = \left(\mu_2^r - 1\right)\mathbf{H}(\bar{r}) = \left(\mu_2^r - 1\right)J_s\,\hat{\mathbf{z}} \cong \mu_2^r\,J_s\,\hat{\mathbf{z}} \quad A/m$$

$$\mathbf{J}_a^{sm}(\bar{r}) = \mathbf{M}_2(\bar{r})\times\hat{\mathbf{n}} = \mu_2^r J_s\,\hat{\mathbf{z}}\times\hat{\boldsymbol{\rho}} = \mu_2^r\,J_s\,\hat{\boldsymbol{\varphi}} \quad A/m$$

$$\mathbf{J}_b^{sm}(\bar{r}) = \mathbf{M}_1(\bar{r})\times\hat{\mathbf{n}} = \mu_1^r J_s\,\hat{\mathbf{z}}\times\left(-\hat{\boldsymbol{\rho}}\right) = -\mu_1^r\,J_s\,\hat{\boldsymbol{\varphi}} \quad A/m$$

$$\mathbf{J}_c^{sm}(\bar{r}) = \mathbf{M}_1(\bar{r})\times\hat{\mathbf{n}} = \mu_1^r J_s\,\hat{\mathbf{z}}\times\hat{\boldsymbol{\rho}} = \mu_1^r\,J_s\,\hat{\boldsymbol{\varphi}} \quad A/m$$

$$\mathbf{B}(\bar{r}) = \frac{\mu_0}{4\pi}\iint_S \frac{\mathbf{J}_s(\bar{r}')\times(\bar{r}-\bar{r}')}{|\bar{r}-\bar{r}'|^3}\,ds'$$

$$= \frac{\mu_0}{4\pi}J_{sm}\int_0^{2\pi}\int_{-\infty}^{0}\frac{\hat{\boldsymbol{\varphi}}'\times(\bar{r}-\bar{r}')}{|\bar{r}-\bar{r}'|^3}\,dz'\,a\,d\varphi'$$

'r' is the direction of the particle, Jsm is the summation of the surface currents for each of the corresponding cylinders

$$\bar{r} = x\,\hat{\mathbf{x}} + y\,\hat{\mathbf{y}} + z\,\hat{\mathbf{z}}$$

'a' is the radius of each cylinder. One set of equations for each corresponding current: on glue, inside core, outside core.

$$\bar{r}' = a\cos\varphi'\,\hat{\mathbf{x}} + a\sin\varphi'\,\hat{\mathbf{y}} + z'\,\hat{\mathbf{z}}$$

$$\bar{r} - \bar{r}' = \left(x - a\cos\varphi'\right)\hat{\mathbf{x}} + \left(y - a\sin\varphi'\right)\hat{\mathbf{y}} + \left(z - z'\right)\hat{\mathbf{z}}$$

$$\left|\bar{r} - \bar{r}'\right|^{-3} = \left[\left(x - a\cos\varphi'\right)^2 + \left(y - a\sin\varphi'\right)^2 + \left(z - z'\right)^2\right]^{-3/2}$$

$$\begin{aligned}\hat{\boldsymbol{\varphi}}' \times \left(\bar{r} - \bar{r}'\right) &= \left(x - a\cos\varphi'\right)\hat{\boldsymbol{\varphi}}' \times \hat{\mathbf{x}} \\ &+ \left(y - a\sin\varphi'\right)\hat{\boldsymbol{\varphi}}' \times \hat{\mathbf{y}} \\ &+ \left(z - z'\right)\hat{\boldsymbol{\varphi}}' \times \hat{\mathbf{z}}\end{aligned}$$

Solving for the numerator of B(r)

$$\hat{\boldsymbol{\varphi}}' = -\sin\varphi'\,\hat{\mathbf{x}} + \cos\varphi'\,\hat{\mathbf{y}}$$

Definition of the unit vector φ

$$\begin{aligned}\hat{\boldsymbol{\varphi}}' \times \hat{\mathbf{x}} &= -\sin\varphi'\,\hat{\mathbf{x}} \times \hat{\mathbf{x}} + \cos\varphi'\,\hat{\mathbf{y}} \times \hat{\mathbf{x}} \\ &= -\cos\varphi'\,\hat{\mathbf{z}}\end{aligned}$$

Cross-products in the numerator of B(r)

$$\hat{\boldsymbol{\varphi}}' \times \hat{\mathbf{y}} = -\sin\varphi'\ \hat{\mathbf{x}} \times \hat{\mathbf{y}} + \cos\varphi'\ \hat{\mathbf{y}} \times \hat{\mathbf{y}}$$
$$= -\sin\varphi'\ \hat{\mathbf{z}}$$

$$\hat{\boldsymbol{\varphi}}' \times \hat{\mathbf{z}} = -\sin\varphi'\ \hat{\mathbf{x}} \times \hat{\mathbf{z}} + \cos\varphi'\ \hat{\mathbf{y}} \times \hat{\mathbf{z}}$$
$$= \sin\varphi'\ \hat{\mathbf{y}} + \cos\varphi'\ \hat{\mathbf{x}}$$

$$\hat{\boldsymbol{\varphi}}' \times (\bar{r} - \bar{r}') = -\left(x\cos\varphi' - a\cos^2\varphi'\right)\ \hat{\mathbf{z}}$$
$$- \left(y\sin\varphi' - a\sin^2\varphi'\right)\ \hat{\mathbf{z}}$$
$$+ \left(z - z'\right)\sin\varphi'\ \hat{\mathbf{y}} + \left(z - z'\right)\cos\varphi'\ \hat{\mathbf{x}}$$
$$= \left(a - x\cos\varphi' - y\sin\varphi'\right)\ \hat{\mathbf{z}}$$
$$+ \left(z - z'\right)\sin\varphi'\ \hat{\mathbf{y}} + \left(z - z'\right)\cos\varphi'\ \hat{\mathbf{x}}$$

$$\left|\bar{r} - \bar{r}'\right|^{-3} = \left[\left(x - a\cos\varphi'\right)^2 + \left(y - a\sin\varphi'\right)^2 + \left(z - z'\right)^2\right]^{-3/2}$$
$$= \left[\beta^2 + \left(z - z'\right)^2\right]^{-3/2}$$

Substitution

$$\beta^2 \;=\; \left(x - a\cos\varphi'\right)^2 \;+\; \left(y - a\sin\varphi'\right)^2$$

$$\int_{-\infty}^{0} \frac{\hat{\boldsymbol{\varphi}}' \times \left(\bar{r} - \bar{r}'\right)}{\left|\bar{r} - \bar{r}'\right|^3}\, dz'$$

Integrating using above cross-product solutions

$$= \left(a - x\cos\varphi' - y\sin\varphi'\right)\, \hat{\mathbf{z}} \int_{-\infty}^{0} \left[\beta^2 \;+\; \left(z - z'\right)^2\right]^{-3/2} dz'$$

$$+ \left(\sin\varphi'\, \hat{\mathbf{y}} \;+\; \cos\varphi'\, \hat{\mathbf{x}}\right) \int_{-\infty}^{0} \left(z - z'\right)\left[\beta^2 \;+\; \left(z - z'\right)^2\right]^{-3/2} dz'$$

Equation 1

$$\int_{-\infty}^{0} \left[\beta^2 + \left(z - z'\right)^2\right]^{-3/2} dz' \;=\; \int_{+\infty}^{z} \left[\beta^2 + u^2\right]^{-3/2} \left(-du\right)$$

$$= \int_{z}^{+\infty} \left[\beta^2 + u^2\right]^{-3/2} du$$

$$= \Big|_{z}^{\infty} u\left(1 + \frac{u^2}{\beta^2}\right)\left[\beta^2 + u^2\right]^{-3/2}$$

$$= \frac{1}{\beta^2} - z\left(1 + \frac{z^2}{\beta^2}\right)\left[\beta^2 + z^2\right]^{-3/2}$$

$$= \frac{1}{\beta^2}\left[1 - z\left(\beta^2 + z^2\right)^{-1/2}\right]$$

Equation 2

$$\int_{-\infty}^{0} (z - z')\left[\beta^2 + (z - z')^2\right]^{-3/2} dz' = \int_{+\infty}^{z} u\left[\beta^2 + u^2\right]^{-3/2}(-du)$$

$$= \int_{z}^{+\infty} u\left[\beta^2 + u^2\right]^{-3/2} du$$

$$= \Big|_{z}^{\infty} -\left[\beta^2 + u^2\right]^{-1/2}$$

$$= \left[\beta^2 + z^2\right]^{-1/2}$$

Combining the results of 1 & 2 become this

$$\int_{-\infty}^{0} \frac{\hat{\boldsymbol{\varphi}}' \times (\bar{r} - \bar{r}')}{|\bar{r} - \bar{r}'|^3} dz'$$

$$= \left(a - x\cos\varphi' - y\sin\varphi'\right)\ \hat{\mathbf{z}}\ \frac{1}{\beta^2}\left[1 - z\left(\beta^2 + z^2\right)^{-1/2}\right]$$

$$+ \left(\sin\varphi'\,\hat{\mathbf{y}} + \cos\varphi'\,\hat{\mathbf{x}}\right)\left[\beta^2 + z^2\right]^{-1/2}$$

Solving for the second integral using the previous result

Equation 3

$$\int_0^{2\pi}\int_{-\infty}^{0} \frac{\hat{\boldsymbol{\varphi}}' \times (\bar{r} - \bar{r}')}{|\bar{r} - \bar{r}'|^3} = \hat{\mathbf{z}} \int_0^{2\pi} (a - x\cos\varphi' - y\sin\varphi') \frac{1}{\beta^2}\left[1 - z\left(\beta^2 + z^2\right)^{-1/2}\right] a\, d\varphi'$$

$$+ \hat{\mathbf{x}} \int_0^{2\pi} \cos\varphi' \left[\beta^2 + z^2\right]^{-1/2} a\, d\varphi'$$

$$+ \hat{\mathbf{y}} \int_0^{2\pi} \sin\varphi' \left[\beta^2 + z^2\right]^{-1/2} a\, d\varphi'$$

$G_1$ is defined by this substitution. Has no closed form solution, so must use Taylor series expansion

$$g_1(\bar{r}, \varphi') \doteq \left[\beta^2 + z^2\right]^{-1/2}$$

$$= \left[\left(x - a\cos\varphi'\right)^2 + \left(y - a\sin\varphi'\right)^2 + z^2\right]^{-1/2}$$

Taylor series expansion around a. Assumes x,y,z>>a. Truncated at 4 terms.

$$\cong \frac{1}{r} + a\left(\frac{x}{r^3}\right)\cos\varphi' + a\left(\frac{y}{r^3}\right)\sin\varphi'$$

$$+ a^2\left(1.5\frac{x^2}{r^5}\right)\cos^2\varphi' + a^2\left(1.5\frac{y^2}{r^5}\right)\sin^2\varphi'$$

$$+ a^2\left(3.0\frac{x\,y}{r^5}\right)\sin\varphi'\cos\varphi' - a^2\left(\frac{0.5}{r^3}\right)$$

$$- a^3\left(1.5\frac{x}{r^5}\right)\cos\varphi' - a^3\left(1.5\frac{y}{r^5}\right)\sin\varphi'$$

$$+ a^3\left(2.5\frac{x^3}{r^7}\right)\cos^3\varphi' + a^3\left(7.5\frac{x^2\,y}{r^7}\right)\cos^2\varphi'\sin\varphi'$$

$$+ a^3\left(7.5\frac{x\,y^2}{r^7}\right)\cos\varphi'\sin^2\varphi' + a^3\left(2.5\frac{y^3}{r^7}\right)\sin^3\varphi'$$

$$\int_0^{2\pi} \sin\varphi'\; g_1(\bar{r},\varphi')\, a\, d\varphi'$$

Substitute Taylor Series back into the outside integral and simplify

$$= + \pi a^2 \left(\frac{y}{r^3}\right) - \pi a^4 \left(1.5\frac{y}{r^5}\right) + \pi a^4 \left(\frac{7.5}{4}\frac{x^2\, y}{r^7}\right) + \pi a^4 \left(\frac{7.5}{4}\frac{y^3}{r^7}\right)$$

$$= + \pi a^2 \left(\frac{y}{r^3}\right) - \pi a^4 \left(1.5\frac{y}{r^5}\right) + \pi a^4 \left(\frac{7.5}{4}\frac{\rho^2\, y}{r^7}\right)$$

$$\int_0^{2\pi} \cos\varphi'\; g_1\left(\bar{r},\varphi'\right) a\, d\varphi'$$

$$= + \pi a^2 \left(\frac{x}{r^3}\right) - \pi a^4 \left(1.5\frac{x}{r^5}\right)$$

$$+ \pi a^4 \left(\frac{7.5}{4}\frac{y^2\, x}{r^7}\right)$$

$$+ \pi a^4 \left(\frac{7.5}{4}\frac{x^3}{r^7}\right)$$

$$= \pi a^2 \left(\frac{x}{r^3}\right) - \pi a^4 \left(1.5\frac{x}{r^5}\right)$$

$$+ \pi a^4 \left(\frac{7.5}{4}\frac{\rho^2\, x}{r^7}\right)$$

Repeat for cosine component: Substitute Taylor Series back into the outside integral and simplify

$$\hat{\mathbf{x}} \int_0^{2\pi} \cos\varphi' \; g_1(\bar{r},\varphi')\, a \; d\varphi' \; + \; \hat{\mathbf{y}} \int_0^{2\pi} \sin\varphi' \; g_1(\bar{r},\varphi')\, a \; d\varphi'$$

$$= \hat{\mathbf{x}} \left( \pi a^2 \left( \frac{x}{r^3} \right) - \; \pi a^4 \left( 1.5 \frac{x}{r^5} \right) \; + \; \pi a^4 \left( \frac{7.5}{4} \frac{\rho^2 \; x}{r^7} \right) \right)$$

$$+ \hat{\mathbf{y}} \left( \pi a^2 \left( \frac{y}{r^3} \right) - \; \pi a^4 \left( 1.5 \frac{y}{r^5} \right) \; + \; \pi a^4 \left( \frac{7.5}{4} \frac{\rho^2 \; y}{r^7} \right) \right)$$

$$= \left( x \; \hat{\mathbf{x}} + y \; \hat{\mathbf{y}} \right) \left( \pi a^2 \left( \frac{1}{r^3} \right) - \; \pi a^4 \left( 1.5 \frac{1}{r^5} \right) \; + \; \pi a^4 \left( \frac{7.5}{4} \frac{\rho^2}{r^7} \right) \right)$$

$$= \hat{\boldsymbol{\rho}} \rho \left( \pi a^2 \left( \frac{1}{r^3} \right) - \; \pi a^4 \left( 1.5 \frac{1}{r^5} \right) \; + \; \pi a^4 \left( \frac{7.5}{4} \frac{\rho^2}{r^7} \right) \right)$$

$$= \hat{\boldsymbol{\rho}} \left( \pi a^2 \left( \frac{\rho}{r^3} \right) - \; \pi a^4 \left( 1.5 \frac{\rho}{r^5} \right) \; + \; \pi a^4 \left( \frac{7.5}{4} \frac{\rho^3}{r^7} \right) \right)$$

Adding the results of the two (sin & cos) components back together results in this final solution

$$\rho = r \sin\theta \qquad z = r \cos\theta$$

$$x = \rho \cos\varphi = r \sin\theta \cos\varphi$$

Substitutions for coordinate system

$$y = \rho \sin\varphi = r \sin\theta \sin\varphi$$

$$\hat{\mathbf{x}} \int_0^{2\pi} \cos\varphi' \; g_1(\bar{r},\varphi')\, a \, d\varphi' \; + \; \hat{\mathbf{y}} \int_0^{2\pi} \sin\varphi' \; g_1(\bar{r},\varphi')\, a \, d\varphi'$$

$$= \hat{\boldsymbol{\rho}} \left( \pi a^2 \left( \frac{\rho}{r^3} \right) - \; \pi a^4 \left( 1.5 \frac{\rho}{r^5} \right) \; + \; \pi a^4 \left( \frac{7.5}{4} \frac{\rho^3}{r^7} \right) \right)$$

$$= \hat{\boldsymbol{\rho}} \left( \pi a^2 \left( \frac{1}{r^2} \sin\theta \right) - \; \pi a^4 \left( 1.5 \frac{1}{r^4} \sin\theta \right) \; + \; \pi a^4 \left( \frac{7.5}{4} \frac{1}{r^4} \sin^3\theta \right) \right)$$

Simplified solution with substitutions

$$g_2(\bar{r},\varphi') \;\doteq\; \frac{1}{\beta^2}\left[ 1 - z\left(\beta^2 + z^2\right)^{-1/2} \right]$$

$$\cong \; g_2^{0th}(\bar{r},\varphi') \; + \; g_2^{1st}(\bar{r},\varphi') \; + \; g_2^{2nd}(\bar{r},\varphi') \; + \; g_2^{3rd}(\bar{r},\varphi')$$

New g substitution for the z component in equation 3

$$g_2^{0th}(\bar{r},\varphi') = \frac{1}{\rho^2}\left(1-\frac{z}{r}\right)$$

Taylor series approximation for $g_2$ divided into individual terms as described in the previous equation

$$g_2^{1st}(\bar{r},\varphi') = a\frac{2}{\rho^4}\left(1-\frac{z}{r}\right)\left(x\cos\varphi'+y\sin\varphi'\right)$$
$$-a\frac{z}{\rho^2 r^3}\left(x\cos\varphi'+y\sin\varphi'\right)$$
$$= \frac{a}{\rho^2}\left(x\cos\varphi'+y\sin\varphi'\right)\left(\frac{2}{\rho^2}-2\frac{z}{\rho^2 r}-\frac{z}{r^3}\right)$$

$$g_2^{2nd}(\bar{r},\varphi) = \frac{a^2}{\rho^6}\left(1-\frac{z}{r}\right)$$
$$\left(\left(3x^2-y^2\right)\cos^2\varphi'+8xy\cos\varphi'\sin\varphi'+\left(3y^2-x^2\right)\sin^2\varphi'\right)$$
$$-a^2\frac{2z}{\rho^4 r^3}\left(x\cos\varphi'+y\sin\varphi'\right)^2$$
$$-1.5a^2\frac{z}{\rho^2 r^5}\left(x\cos\varphi'+y\sin\varphi'\right)^2$$
$$+0.5a^2\frac{z}{\rho^2 r^3}$$

$$
\begin{aligned}
g_2^{3rd}(\bar{r},\varphi) \;=\;& -a^3\frac{z}{\rho^6 r^3}\left(x\cos\varphi' + y\sin\varphi'\right)\\
&\left(\left(3x^2-y^2\right)\cos^2\varphi' + 8xy\cos\varphi'\sin\varphi' + \left(3y^2-x^2\right)\sin^2\varphi'\right)\\
&+a^3\frac{4}{\rho^8}\left(1-\frac{z}{r}\right)\\
&\left(\left(x^3-xy^2\right)\cos^3\varphi' + \left(5x^2y-y^3\right)\cos^2\varphi'\sin\varphi' + \left(5xy^2-x^3\right)\cos\varphi'\sin^2\varphi' + \left(y^3-x^2y\right)\sin^3\varphi'\right)\\
&-a^3\frac{3z}{\rho^4 r^5}\left(x\cos\varphi' + y\sin\varphi'\right)^3\\
&+a^3\frac{z}{\rho^4 r^3}\left(x\cos\varphi' + y\sin\varphi'\right)\\
&-a^3 2.5\frac{z}{\rho^2 r^7}\left(x\cos\varphi' + y\sin\varphi'\right)^3\\
&+a^3 1.5\frac{z}{\rho^2 r^5}\left(x\cos\varphi' + y\sin\varphi'\right)
\end{aligned}
$$

Simplification

$$
\begin{aligned}
&\left(3x^2-y^2\right)\cos^2\varphi' + 8xy\cos\varphi'\sin\varphi' + \left(3y^2-x^2\right)\sin^2\varphi'\\
&= \left(4x^2-x^2-y^2\right)\cos^2\varphi' + 8xy\cos\varphi'\sin\varphi' + \left(4y^2-y^2-x^2\right)\sin^2\varphi'\\
&= \left(4x^2\right)\cos^2\varphi' + 8xy\cos\varphi'\sin\varphi' + \left(4y^2\right)\sin^2\varphi'\\
&+\left(-x^2-y^2\right)\cos^2\varphi' + \left(-y^2-x^2\right)\sin^2\varphi'\\
&= \left(2x\cos\varphi' + 2y\sin\varphi'\right)^2 - \left(x^2+y^2\right)\\
&= 4\left(x\cos\varphi' + y\sin\varphi'\right)^2 - \left(x^2+y^2\right)
\end{aligned}
$$

$$\left(x^3 - xy^2\right)\cos^3\varphi' + \left(5x^2y - y^3\right)\cos^2\varphi'\sin\varphi' + \left(5xy^2 - x^3\right)\cos\varphi'\sin^2\varphi' + \left(y^3 - x^2y\right)\sin^3\varphi'$$
$$= \left(x^3\right)\cos^3\varphi' + \left(3x^2y\right)\cos^2\varphi'\sin\varphi' + \left(3xy^2\right)\cos\varphi'\sin^2\varphi' + \left(y^3\right)\sin^3\varphi'$$
$$+ \left(-xy^2\right)\cos^3\varphi' + \left(2x^2y - y^3\right)\cos^2\varphi'\sin\varphi' + \left(2xy^2 - x^3\right)\cos\varphi'\sin^2\varphi' + \left(-x^2y\right)\sin^3\varphi'$$
$$= \left(3x^3 - xy^2\right)\cos^3\varphi' + \left(11x^2y - y^3\right)\cos^2\varphi'\sin\varphi' + \left(11xy^2 - x^3\right)\cos\varphi'\sin^2\varphi' + \left(3y^3 - x^2y\right)\sin^3\varphi'$$
$$+ \left(-2x^3\right)\cos^3\varphi' + \left(-6x^2y\right)\cos^2\varphi'\sin\varphi' + \left(-6xy^2\right)\cos\varphi'\sin^2\varphi' + \left(-2y^3\right)\sin^3\varphi'$$
$$= \left(3x^3 - xy^2\right)\cos^3\varphi' + \left(11x^2y - y^3\right)\cos^2\varphi'\sin\varphi' + \left(11xy^2 - x^3\right)\cos\varphi'\sin^2\varphi' + \left(3y^3 - x^2y\right)\sin^3\varphi'$$
$$-2\left(x^3\cos^3\varphi' + 3x^2y\cos^2\varphi'\sin\varphi' + 3xy^2\cos\varphi'\sin^2\varphi' + y^3\sin^3\varphi'\right)$$
$$= 4\left(x\cos\varphi' + y\sin\varphi'\right)^3 - \left(x^2 + y^2\right)\left(x\cos\varphi' + y\sin\varphi'\right) - 2\left(x\cos\varphi' + y\sin\varphi'\right)^3$$
$$= 2\left(x\cos\varphi' + y\sin\varphi'\right)^3 - \left(x^2 + y^2\right)\left(x\cos\varphi' + y\sin\varphi'\right)$$

| Simplification |
|---|

$$g_2^{2nd}(\bar{r},\varphi) = \frac{a^2}{\rho^6}\left(1-\frac{z}{r}\right)\left(4\left(x\cos\varphi'+y\sin\varphi'\right)^2-\left(x^2+y^2\right)\right)$$

Simplification

$$-a^2\frac{2z}{\rho^4 r^3}\left(x\cos\varphi'+y\sin\varphi'\right)^2$$

$$-a^2 1.5\frac{z}{\rho^2 r^5}\left(x\cos\varphi'+y\sin\varphi'\right)^2$$

$$+a^2 0.5\frac{z}{\rho^2 r^3}$$

$$= \frac{a^2}{\rho^6}\left(1-\frac{z}{r}\right)\left(4\left(x\cos\varphi'+y\sin\varphi'\right)^2\right)$$

$$-a^2\frac{2z}{\rho^4 r^3}\left(x\cos\varphi'+y\sin\varphi'\right)^2$$

$$-1.5a^2\frac{z}{\rho^2 r^5}\left(x\cos\varphi'+y\sin\varphi'\right)^2$$

$$+0.5a^2\frac{z}{\rho^2 r^3}$$

$$-\frac{a^2}{\rho^4}\left(1-\frac{z}{r}\right)$$

$$= a^2\left(\frac{4}{\rho^6}\left(1-\frac{z}{r}\right)-\frac{2z}{\rho^4 r^3}-1.5\frac{z}{\rho^2 r^5}\right)\left(x\cos\varphi'+y\sin\varphi'\right)^2$$

$$+0.5a^2\frac{z}{\rho^2 r^3}-\frac{1}{\rho^4}\left(1-\frac{z}{r}\right)$$

$$
\begin{aligned}
g_2^{3rd}(\bar{r},\varphi) \quad = \quad & -a^3\frac{z}{\rho^6 r^3}\left(x\cos\varphi' + y\sin\varphi'\right) \\
& \left(4\left(x\cos\varphi' + y\sin\varphi'\right)^2 - \left(x^2+y^2\right)\right) \\
& +a^3\frac{4}{\rho^8}\left(1-\frac{z}{r}\right) \\
& \left(2\left(x\cos\varphi' + y\sin\varphi'\right)^3 - \left(x^2+y^2\right)\left(x\cos\varphi' + y\sin\varphi'\right)\right) \\
& -a^3\frac{3z}{\rho^4 r^5}\left(x\cos\varphi' + y\sin\varphi'\right)^3 \\
& +a^3\frac{z}{\rho^4 r^3}\left(x\cos\varphi' + y\sin\varphi'\right) \\
& -a^3 2.5\frac{z}{\rho^2 r^7}\left(x\cos\varphi' + y\sin\varphi'\right)^3 \\
& +a^3 1.5\frac{z}{\rho^2 r^5}\left(x\cos\varphi' + y\sin\varphi'\right) \\
= \quad & -a^3\frac{4z}{\rho^6 r^3}\left(x\cos\varphi' + y\sin\varphi'\right)^3 \\
& +a^3\frac{z}{\rho^4 r^3}\left(x\cos\varphi' + y\sin\varphi'\right) \\
& +a^3\frac{8}{\rho^8}\left(1-\frac{z}{r}\right)\left(x\cos\varphi' + y\sin\varphi'\right)^3 \\
& -a^3\frac{4}{\rho^6}\left(1-\frac{z}{r}\right)\left(x\cos\varphi' + y\sin\varphi'\right) \\
& -a^3\frac{3z}{\rho^4 r^5}\left(x\cos\varphi' + y\sin\varphi'\right)^3 \\
& +a^3\frac{z}{\rho^4 r^3}\left(x\cos\varphi' + y\sin\varphi'\right) \\
& -a^3 2.5\frac{z}{\rho^2 r^7}\left(x\cos\varphi' + y\sin\varphi'\right)^3 \\
& +a^3 1.5\frac{z}{\rho^2 r^5}\left(x\cos\varphi' + y\sin\varphi'\right)
\end{aligned}
$$

Simplification

$$g_2^{3rd}(\bar{r},\varphi) = a^3\left(\frac{8}{\rho^8}\left(1-\frac{z}{r}\right)-\frac{4z}{\rho^6 r^3}-\frac{3z}{\rho^4 r^5}-2.5\frac{z}{\rho^2 r^7}\right)\left(x\cos\varphi'+y\sin\varphi'\right)^3$$
$$+a^3\left(-\frac{4}{\rho^6}\left(1-\frac{z}{r}\right)+\frac{2z}{\rho^4 r^3}+1.5\frac{z}{\rho^2 r^5}\right)\left(x\cos\varphi'+y\sin\varphi'\right)$$

Integration over φ

$$\int_0^{2\pi}\left(x\cos\varphi'+y\sin\varphi'\right)^1 d\varphi = 0$$

$$\int_0^{2\pi}\left(x\cos\varphi'+y\sin\varphi'\right)^2 d\varphi = \pi\rho^2$$

$$\int_0^{2\pi}\left(x\cos\varphi'+y\sin\varphi'\right)^3 d\varphi = 0$$

6 fundamental integral parts all in terms of equation 3

$$\int_0^{2\pi} x\cos\varphi'\left(x\cos\varphi'+y\sin\varphi'\right)^1 d\varphi = \pi x^2$$

$$\int_0^{2\pi} x\cos\varphi'\left(x\cos\varphi'+y\sin\varphi'\right)^2 d\varphi = 0$$

$$\int_0^{2\pi} x\cos\varphi'\left(x\cos\varphi'+y\sin\varphi'\right)^3 d\varphi = \pi\frac{3}{4}x^2\rho^2$$

Using result of 1st component simplification and substitutions to integrate over φ

$$\int_0^{2\pi}\left(a-x\cos\varphi'-y\sin\varphi'\right)\frac{1}{\beta^2}\left[1-z\left(\beta^2+z^2\right)^{-1/2}\right]a\,d\varphi'$$

$$\int_0^{2\pi} a\, g_2^{0th}(\bar{r},\varphi')\, a\, d\varphi' \quad = \quad \pi a^2 \frac{2}{\rho^2}\left(1-\frac{z}{r}\right)$$

Integrate over φ for all components to solve 2nd integral

$$\int_0^{2\pi} a\, g_2^{1st}(\bar{r},\varphi')\, a\, d\varphi' \quad = \quad 0$$

$$\begin{aligned}\int_0^{2\pi} a\, g_2^{2nd}(\bar{r},\varphi')\, a\, d\varphi' \quad &= \quad \pi a^4\left(\frac{4}{\rho^4}\left(1-\frac{z}{r}\right)-\frac{2z}{\rho^2 r^3}-1.5\frac{z}{r^5}\right)\\ &+ \quad \pi a^4\left(\frac{z}{\rho^2 r^3}-\frac{1}{\rho^4}\left(1-\frac{z}{r}\right)\right)\\ &= \quad \pi a^4\left(\frac{3}{\rho^4}\left(1-\frac{z}{r}\right)+\frac{2z}{\rho^2 r^3}-1.5\frac{z}{r^5}\right)\end{aligned}$$

$$\int_0^{2\pi} a\, g_2^{3rd}(\bar{r},\varphi')\, a\, d\varphi' \quad = \quad 0$$

$$\int_0^{2\pi} -\left(x\cos\varphi' + y\sin\varphi'\right) g_2^{0th}(\bar{r},\varphi')\, a\, d\varphi' \quad = \quad 0$$

$$\int_0^{2\pi} -\left(x\cos\varphi' + y\sin\varphi'\right) g_2^{1th}\left(\bar{r},\varphi'\right) a\, d\varphi' = \pi a^2\left(\frac{z}{r^3} + 2\frac{z}{\rho^2 r} - \frac{2}{\rho^2}\right)$$

$$= \pi a^2\left(\frac{z}{r^3} - \frac{2}{\rho^2}\left(1 - \frac{z}{r}\right)\right)$$

$$\int_0^{2\pi} -\left(x\cos\varphi' + y\sin\varphi'\right) g_2^{2nd}\left(\bar{r},\varphi'\right) a\, d\varphi' = 0$$

$$\int_0^{2\pi} -\left(x\cos\varphi' + y\sin\varphi'\right) g_2^{3rd}\left(\bar{r},\varphi'\right) a\, d\varphi'$$

$$= \pi a^4 \frac{3}{4}\left(-\frac{8}{\rho^4}\left(1 - \frac{z}{r}\right) + \frac{4z}{\rho^2 r^3} + \frac{3z}{r^5} + 2.5\frac{z\,\rho^2}{r^7}\right)$$

$$+\pi a^4\left(\frac{4}{\rho^4}\left(1 - \frac{z}{r}\right) - \frac{2z}{\rho^2 r^3} - 1.5\frac{z}{r^5}\right)$$

$$= \pi a^4\left(-\frac{6}{\rho^4}\left(1 - \frac{z}{r}\right) + \frac{3z}{\rho^2 r^3} + 2.25\frac{z}{r^5} + 1.875\frac{z\,\rho^2}{r^7}\right)$$

$$+\pi a^4\left(\frac{4}{\rho^4}\left(1 - \frac{z}{r}\right) - \frac{2z}{\rho^2 r^3} - 1.5\frac{z}{r^5}\right)$$

$$= \pi a^4\left(-\frac{2}{\rho^4}\left(1 - \frac{z}{r}\right) + \frac{z}{\rho^2 r^3} + 0.75\frac{z}{r^5} + 1.875\frac{z\,\rho^2}{r^7}\right)$$

$$\int_0^{2\pi} \left(a - x\cos\varphi' - y\sin\varphi'\right)\frac{1}{\beta^2}\left[1 - z\left(\beta^2 + z^2\right)^{-1/2}\right] a\, d\varphi'$$

$$= \pi a^2 \frac{2}{\rho^2}\left(1 - \frac{z}{r}\right)$$

$$+\pi a^2\left(\frac{z}{r^3} - \frac{2}{\rho^2}\left(1 - \frac{z}{r}\right)\right)$$

$$+\pi a^4\left(\frac{3}{\rho^4}\left(1 - \frac{z}{r}\right) + \frac{2z}{\rho^2 r^3} - 1.5\frac{z}{r^5}\right)$$

$$+\pi a^4\left(-\frac{2}{\rho^4}\left(1 - \frac{z}{r}\right) + \frac{z}{\rho^2 r^3} + 0.75\frac{z}{r^5} + 1.875\frac{z\,\rho^2}{r^7}\right)$$

$$= \pi a^2\left(\frac{z}{r^3}\right)$$

$$+\pi a^4\left(-\frac{2}{\rho^4}\left(1 - \frac{z}{r}\right) + \frac{z}{\rho^2 r^3} - 0.75\frac{z}{r^5} + 1.875\frac{z\,\rho^2}{r^7}\right)$$

$$= \pi\frac{a^2}{\rho^2}\left(\frac{\rho^2 z}{r^3}\right)$$

$$+\pi\frac{a^4}{\rho^4}\left(-2\left(1 - \frac{z}{r}\right) + \frac{\rho^2 z}{r^3} - 0.75\frac{\rho^4 z}{r^5} + 1.875\frac{\rho^6\, z}{r^7}\right)$$

Combining all the integrals into 1 solution

$$\int_0^{2\pi} \left(a - x\cos\varphi' - y\sin\varphi'\right)\frac{1}{\beta^2}\left[1 - z\left(\beta^2 + z^2\right)^{-1/2}\right] a\, d\varphi'$$

$$= \pi\frac{a^2}{\rho^2}\left(\frac{\rho^2 z}{r^3}\right)$$

$$+\pi\frac{a^4}{\rho^4}\left(-2\left(1 - \frac{z}{r}\right) + \frac{\rho^2 z}{r^3} - 0.75\frac{\rho^4 z}{r^5} + 1.875\frac{\rho^6\, z}{r^7}\right)$$

Cylindrical coordinates of the same solution

$$= \pi\frac{a^2}{\rho^2}\left(\sin^2\theta\cos\theta\right)$$

$$+\pi\frac{a^4}{\rho^4}\left(-2\left(1 - \cos\theta\right) + \sin^2\theta\cos\theta - 0.75\sin^4\theta\cos\theta + 1.875\sin^6\theta\cos\theta\right)$$

g1=Bx

Final result of ρ-component of B

$$= \hat{\boldsymbol{\rho}}\left(\pi a^2\left(\frac{\rho}{r^3}\right)\right)$$

$$+\hat{\boldsymbol{\rho}}\left(-\pi a^4\left(1.5\frac{\rho}{r^5}\right) + \pi a^4\left(\frac{7.5}{4}\frac{\rho^3}{r^7}\right)\right)$$

g2=Bz

Final result of z-component of B

$$+\hat{\mathbf{z}}\pi a^2\left(\frac{z}{r^3}\right)$$

$$+\hat{\mathbf{z}}\pi a^4\left(-\frac{2}{\rho^4}\left(1 - \frac{z}{r}\right) + \frac{z}{\rho^2 r^3} - 0.75\frac{z}{r^5} + 1.875\frac{z\,\rho^2}{r^7}\right)$$

Insert these terms back into the original B(r) equation 3. The model uses this result, and the constants that were pulled out $J_s$, $4\pi$ and $\mu_0$ to describe the magnetic flux density provided by the three concentric cylinders. In the model described in chapter 4 only two cylinders are used, the lumen and the iron core. Therefore only two sets of geometric constants (I, N and a) were used. The final result is calculated using each set and added together to describe the full field.

## Appendix B---MATLAB CODE

```
%This script is the determination of the Magnetic force produced
by the
%magnetic field of the solenoid on a particle of given volume.
clear
close all
clc
%% Givens
i=2; %amps
mu0=4*pi*1e-7; %permeability of free space
mu1= 500; %permeability of solenoid core
mu2=50; %permeability of glue---ignore in early model
n_actual=35; %number of turns per 2cm
n=n_actual*50; %number of turns per meter
Js=n*i;
c=0.00386; %meters outermost radius
p=0.00097; %inner radius of core
q=0.0062; %radius of particle (1mL)
v=1E-6; %volume m^3
d=5870; %density of glue kg/m^3
g=9.81; %m/s^2


%% Define Grid
x1=[-10*c:1*c:-c c:1*c:10*c];
z1=[-10*c:1*c:-c c:1*c:10*c];
[x,z] = meshgrid(x1,z1);

rho = x;
r = sqrt(x.^2+z.^2);

%% Find B(r) magnetic flux density
Jsc=mu1.*Js;

Bx_core=(mu0./4.*pi).*((pi.*c.^2.*(rho./r.^3))-
pi.*c.^4.*(1.5.*rho./r.^5)...
    +pi.*c.^4.*(7.5./4.*(rho.^3)./r.^7));
Bz_core=(mu0./4.*pi).*((pi.*c.^2).*(z./(r.^3))+(pi.*c.^4.*(-
2./(rho.^4).*(1-(z./r))...
      +z./(rho.^2.*r.^3)-
0.75.*(z./(r.^5))+1.875.*(z.*rho.^2)./(r.^7))));

Bxc=Jsc.*Bx_core;%magnetic field component x of outer core
current
Bzc=Jsc.*Bz_core;
```

```
Jsp=-mu1.*Js;
Bx_plastic=(mu0./4.*pi).*((pi.*p.^2.*(rho./r.^3))-
pi.*p.^4.*(1.5.*rho./r.^5)...
    +pi.*p.^4.*(7.5./4.*(rho.^3)./r.^7));
Bz_plastic=(mu0./4.*pi).*((pi.*p.^2).*(z./(r.^3))+(pi.*p.^4.*(-
2./(rho.^4).*(1-(z./r))...
      +z./(rho.^2.*r.^3)-
0.75.*(z./(r.^5))+1.875.*(z.*rho.^2)./(r.^7))));
Bxp=Jsp.*Bx_plastic;%inner core current
Bzp=Jsp.*Bz_plastic;

%Plotting for B---sanity check--ok
Bxtotal=Bxc+Bxp;
Bztotal=Bzc+Bzp;
mag=sqrt(Bxtotal.^2+Bztotal.^2);

figure (1)
contourf(x,z,mag)
hold on
quiver(x,z,Bxtotal./mag,Bztotal./mag,'w')
hold off

figure (2)
contourf(x,z,log10(mag))

%% Superposition of two surface currents for each component and
total
Hrho=(Bxtotal)./mu0;
Hz=(Bztotal)./mu0;


%Plotting for H---sanity check, ok
figure (3)
Htotal=sqrt(Hrho.^2+Hz.^2);
contourf(x,z,10.*log10(Htotal))
hold on
quiver(x,z,Hrho./Htotal,Hz./Htotal,'w')
```

Appendix C--- Parametric Analysis Figures

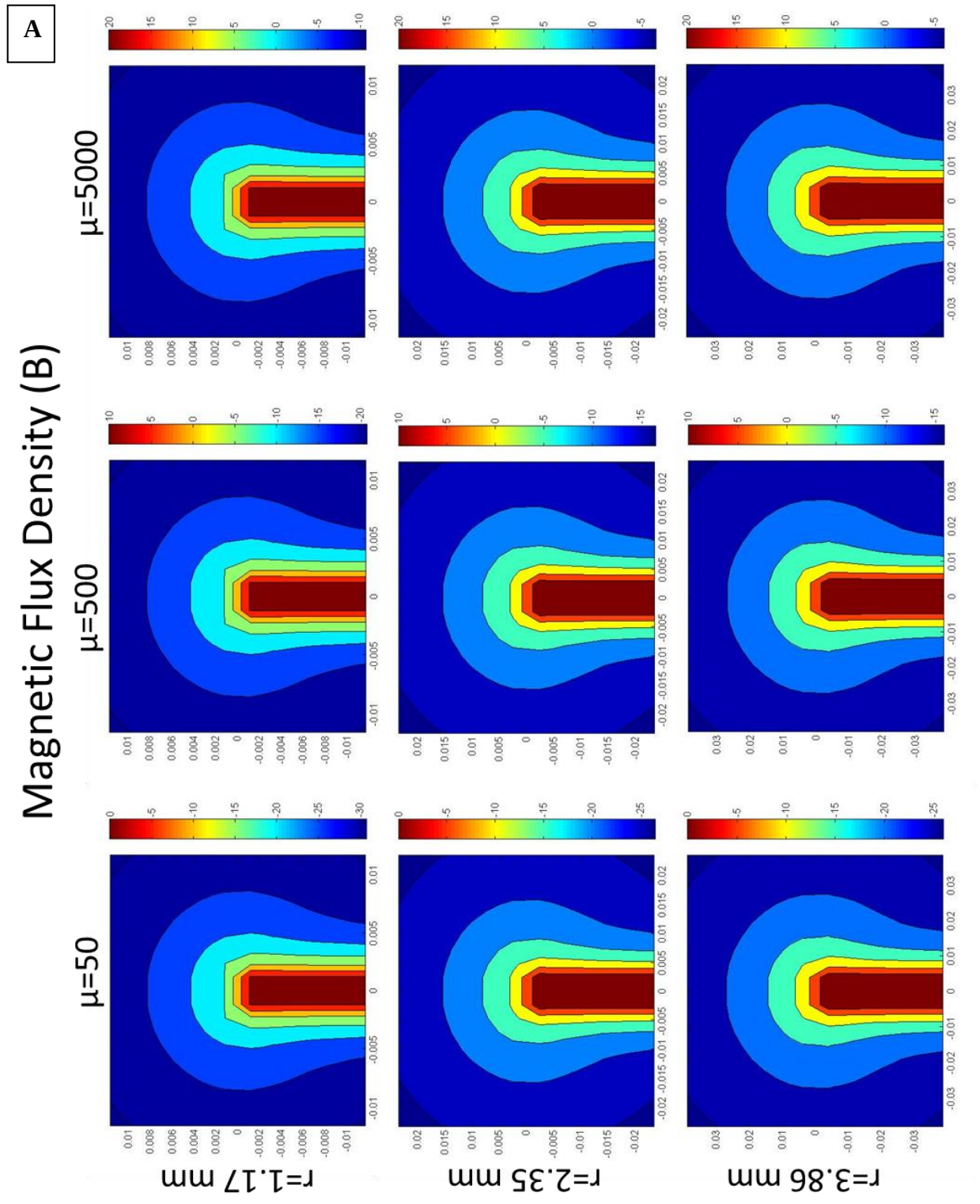

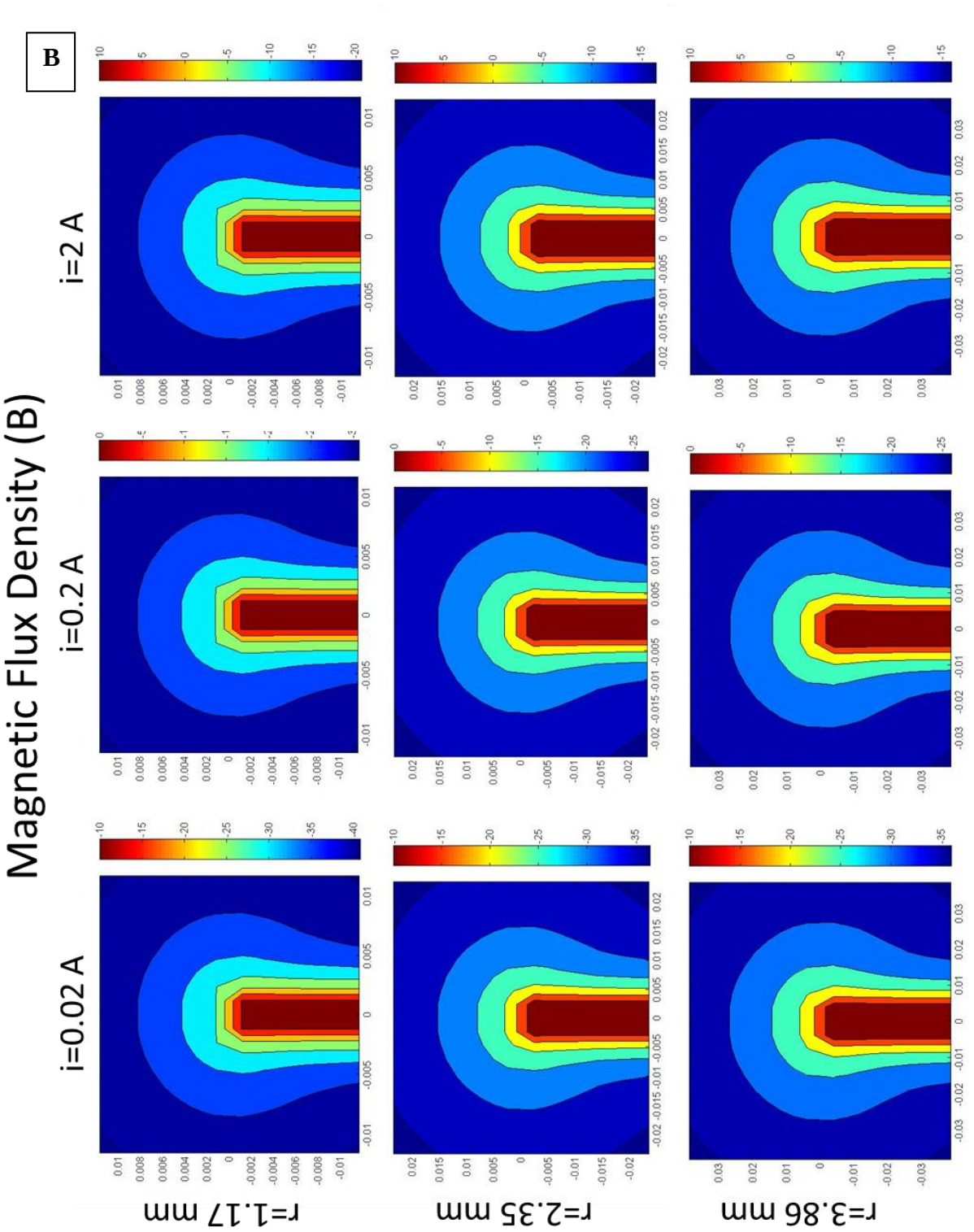


**A---** Parametric analysis of the magnetic flux density. Each plot is shown using spatial dimensions in meters for both the x and z directions. The intensities are shown in the corresponding color bars

directly to the right of each plot. The change from row to row is the radius of the iron core while the change from column to column is the permeability of that core. The current, i, is a constant 2 A for all 9 plots.

**B---** Parametric analysis of the magnetic flux density. Each plot is shown using spatial dimensions in meters for both the x and z directions. The intensities are shown in the corresponding color bars directly to the right of each plot. The change from row to row is the radius of the iron core while the change from column to column is the current applied to the system. The permeability of the core, is a constant of 500.